CHARACTERIZATION OF A PULSATING DRILL BIT BLASTER

By

NICHOLAS JAMES THORP

Bachelor of Science in Mechanical Engineering

Oklahoma State University

Stillwater, Oklahoma

2014

Submitted to the Faculty of the
Graduate College of the
Oklahoma State University in
partial fulfillment of
the requirements for
the Degree of
MASTER OF SCIENCE
May, 2016

CHARACTERIZATION OF A PULSATING DRILL BIT

BLASTER

Thesis Approved:

Thesis Adviser Dr. Geir Hareland

Thesis Co-Advisor Dr. Brian R. Elbing

Dr. Prem K. Bikkina

ACKNOWLEDGEMENTS

This research was supported by Oklahoma State University. We thank Jeff Janzen of NorthBasin Energy Services for the use of the drill bit blaster for testing and research. We also thank the Missouri Institute of Science and Technology for the use of their testing facilities and equipment as well as Dr. Runar Nygaard and Mohammed Al Dushaishi for his help setting up for testing.

Name: NICHOLAS JAMES THORP

Date of Degree: MAY, 2016

Title of Study: CHARACTERIZATION OF A PULSATING DRILL BIT BLASTER

Major Field: MECHANICAL AND AEROSPACE ENGINEERING

Abstract: The drill bit blaster (DBB) studied in this paper aims to maximize the drilling rate of penetration (ROP) by using a flow interrupting mechanism to create drilling fluid pulsation. The fluctuating fluid pressure gradient generated during operation of the DBB could lead to more efficient bit cutting efficiency due to substrate depressurization and increased cutting removal efficiency and the vibrations created could reduce the drill string friction allowing a greater weight on bit (WOB) to be achieved. In order to maximize these mechanisms the effect of several different DBB design changes and operating conditions were studied in above ground testing. An analytical model was created to predict the influence of various aspects of the drill bit blaster design, operating conditions and fluid properties on the bit pressure characteristics and compared against experimental results. The results indicate that internal tool design has a significant effect on the pulsation frequency and amplitude, which can be accurately modeled as a function of flowrate and internal geometry. Using this model an optimization study was conducted to determine the sensitivity of the fluid pulsation power on various design and operating conditions. Application of this technology in future designs could allow the bit pressure oscillation frequency and amplitude to be optimized with regard to the lithology of the formations being drilled which could lead to faster, more efficient drilling, potentially cutting drilling costs and leading to a larger number of oil and natural gas plays being profitable.

TABLE OF CONTENTS

LIST OF TABLES

LIST OF FIGURES

CHAPTER I

INTRODUCTION

There are many natural resources buried deep beneath the Earth that are desirable to bring to the surface. The process by which this is done is known as drilling and the process has evolved dramatically over the past century. Whereas in the past shallow, pressurized resources were primarily targeted, technology has evolved to the point that it is now possible to reach miles below the Earth's surface both vertically and horizontally. This progress has been fueled by fiscal and technological factors continues to this day. For drilling deep wells one of two types of drill bits have traditionally been used: polycrystalline diamond compact (PDC) and roller-cone bits. PDC bits have dozens of hard cutting faces set into the bit face matrix that crush, shear and pulverize the substrate being drilled as the bit rotates. These cuttings are blasted away from the bit face by pressurized drilling fluid which travels through drill pipe from the surface all the way to the bottom of the well under high pressure. Upon exiting the bit face this fluid flushes these cuttings to the annular region between the drill pipe and the well-bore and transports them to the surface of the well. This basic drilling modality has been improved over the past several decades, however there is still significant room for improvement in numerous areas. The drill bit design tested and analyzed in this paper represents another attempt at improving the overall performance of traditional PDC bits by modifying the pressure of the drilling fluid before it exits the bit in a highly controllable and modifiable way using the drill bit blaster (DBB).

1.1 Motivation

Recovering oil and natural gas resources is an efficiency driven process. Often the rate of penetration (ROP) of drilling bottlenecks the entire drilling operation so it is of significant interest within industry to find methods of improving the overall ROP of drilling operations. The DBB studied in this paper creates a pulsating pressure variation within the body of the drill bit by periodically opening then restricting the drilling fluid flow to nozzles, which run through the bit face. These pulsations could lead to an improved ROP through several mechanisms that have been demonstrated to independently increase drilling ROP in laboratory and field testing. Often there is a difficulty in communicating the surface set weight on bit (WOB) down hole through the drill string to the bit due to the friction between the drill string and the wellbore, which reduces the overall ROP as well as introduces uncertainty in surface measurements. It is desirable to have accurate measurements of the WOB during drilling as the ROP is highly dependent on the WOB with both excessively high and excessively low WOBs leading to poor performance and premature failure of the bit. By inducing large enough vibrations both axially and transversely at the bit the friction between the drill string and the wellbore can be reduced as the kinetic friction is less than the static friction. With the increase in popularity of directional wells this could be particularly beneficial as long lateral lengths can only be obtained by minimizing the friction between the drill string and wellbore at the well path dogleg and along the horizontal well section. Another possible ROP improvement mechanism the DBB could create is due to the improved efficiency of bit face cleaning and increased hydraulic impact force due to the vibrations and pressure pulsation. During operation the pressure spikes created by the DBB are higher than the average pressure that would be created without pulsations. An increase in pressure has been linked to higher ROP however there is a limit at which bit pump-off occurs which is a phenomenon in which the pressure generated under the bit by the drilling fluid acting across the bit face exerts a force greater than the WOB and the bit lifts off the bottom of the wellbore

leading to decline or zero ROP. This pressure can be easily calculated as the pressure times the bit face area establishing the maximum pressure drop across the bit that is useable. However, it is possible that by pulsating between pressures higher and lower than this threshold pump-off pressure the ROP could be enhanced either due to the greater maximum pressure usable while avoiding pump-off, or by the repetitive lifting off and slamming down of the bit face onto the substrate being drilled created by the higher and lower parts of the pressure pulsation. Another problematic ROP reducing drilling phenomenon, which occurs in deep wells, is known as the confinement or chip-hold down effect and can decrease the ROP to a fraction of the rate seen during shallow drilling. In deep wells the intense pressure imposed by the drilling fluid column on the bottom of the borehole confines the drilling substrate increasing its compressive strength causing it to become much harder and more difficult to drill. Furthermore, the pressure can cause the substrate to transition from a brittle to a ductile mode of fracture, which further reduces its drillability. Lastly, the constant fluid pressure exerted on the bottom of the borehole by conventional PDC drill bits can hold down cutting chips generated during drilling and lead to a regrinding of cuttings which further reduces the ROP and can lead to a premature wearing out of the drill bit.

The DBB routes the flow of drilling fluid through different nozzles during each cycle of the internal flow interrupter plate, which leads to a depressurization of certain zones under the bit face which could reduce the tendency of the rock to harden as well as enable more efficient transport of fresh cuttings away from the face of the bit. If these ROP improvement mechanisms could be demonstrated with the DBB the reduction in drill time could lead to significant cost savings while drilling and lead to an increased number of oil and natural gas plays being profitable or more profitable. And due to the highly modifiable nature of the pulsation generating mechanism in the DBB the pressure profile frequency, amplitude and waveform shape can be adjusted by varying the geometry of the flow interrupter plate holes. This flexibility could allow

for an interrupter plate selection based on the operational drilling needs and characteristics of the drilling substrate which could lead to an increase in the ROP beyond what has already been demonstrated with previous vibration and pulsation generating designs.

1.2 Drill Bit Blaster Function

The DBB creates fluid pulsations due to the rotation of a circular flow interrupting plate with holes over the fixed internal surface of the bit body as shown in Figs. 1-4. Rotation of the plate is powered by a small diversion of drilling fluid through an internal rotor-stator mud motor within the bit, which connects to the flow interrupter plate by a thin metal rod. The plate sits in a circular depression inside the bit oriented so that the sides of the plate are flush with the inner bit surface and no flow can pass around the plate to the outer bit nozzles. Under the plate are five channels which lead to nozzles on the outside of the bit face; when the interrupter plate rotates the holes in the plate and bit periodically align opening a flow path to an outer nozzle. This change in flow area changes the pressure within the bit increasing the overall bit pressure and creating pressurized pulses of drilling fluid. There are also two central nozzles which are open in such a way that fluid is always able to bypass the flow interrupter plate and pass unrestricted through them. This allows fluid to always exit the bit, albeit at a higher pressure when all the fluid is forced through only the two central nozzles. There is a conical filter covering the interrupter plate with long (2.5 in) slits running lengthwise for the fluid to pass through in order to keep any large pieces of debris away from the interrupter plate and holes. The slant of the conical filter forces any debris down the sides of the filter cone and outward through the central nozzles of the bit, thus bypassing the interrupter plate. There are numerous ways to change the bit design, but the goal of this study was to test the effect of different plate designs on the pulsation performance.

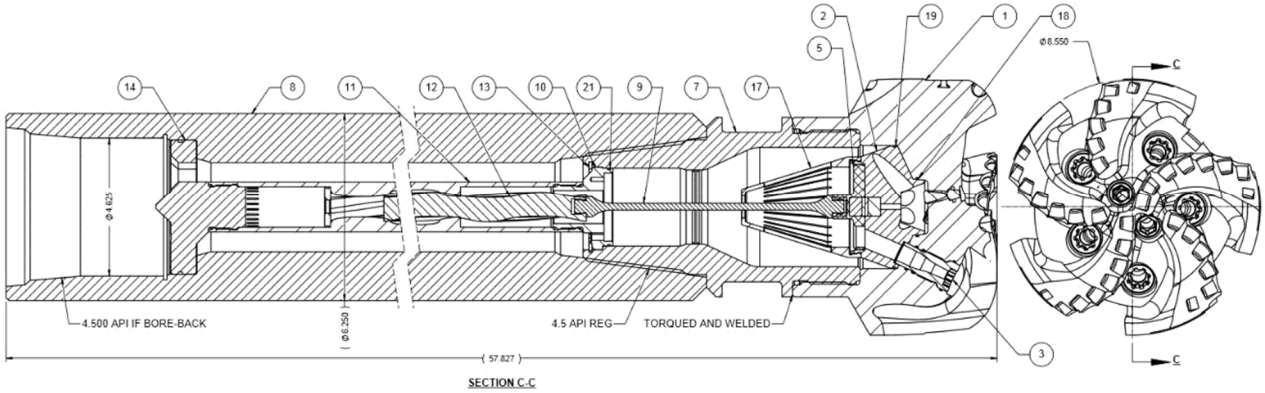

Figure 1: DBB schematic

Figure 2: Face of DBB showing nozzle orientations of outer 5 nozzles and inner 2 nozzles

Figure 3: Internal View of Interrupter Plate Location Showing Nozzle Fluid Paths

Figure 4: Two hole long interrupter plate top (left) and isometric view (right)

CHAPTER II

REVIEW OF LITERATURE

The development of vibrational downhole tools has been a very active field of research, particularly over the past two decades due to the wide spread growth of directional drilling and fracking in the North American oil and gas plays. Due to the long lateral lengths of many of directional fracked wells the maintenance of directional accuracy, ROP and bit life has become increasingly important. The use of vibrational tools has enabled longer lateral lengths due to several performance enhancing mechanisms inherent with the creation of vibration and fluid pulsation along the drill string or at the bit. By vibrating the drill string the coefficient of friction is reduced as the friction is changed from static to kinetic. This frictional change acting over thousands of feet of drillstring leads a significant reduction in the force needed to both drill and pull pipe out of the well. Vibration at the tool face has also been demonstrated to increase the ROP of drilling operations based on the vibrational characteristics of the tool as well as the substrate being drilled. By interrupting the flow to the bit the fluid jet hydraulics can be altered; this impacts the cleaning efficiency of cuttings generated by the bit and can lead to an increase in ROP and bit life as well. Furthermore, by modulating the flow to the bit problems inherent with deep wells like rock confinement induced strengthening and chip-hold down can be mitigated. The benefits of vibrational tools have been demonstrated in the field as well as in the lab. This

review will categorize the available literature by the performance enhancing effect studied as well as describe the function and performance of designs similar to the DBB in order to identify current areas lacking study. By establishing a testing protocol and comparison metric for further vibrational tooling comparisons the mechanisms driving pulsation can be analyzed and the efficacy of this design demonstrated.

2.1 Friction Reduction

Friction is one of the limiting constraints to drilling deeper, longer wells and is particularly limiting in wells which kick-off into a horizontal section. These horizontal wells pose increased frictional problems for two main reasons: the bend of the well and the lateral section of the well (Mirhaj, et al., 2010). At the bend, the drill pipe is forced to deform from a straight shape into that of the curved well path. This compliance is achieved by the elastic deformation of the pipe along a shallow bend radius. However, by bending the pipe in this way the pipe is forced against the sides of the bend with a force proportional to the bending stiffness of the material similar to Fig. 5.

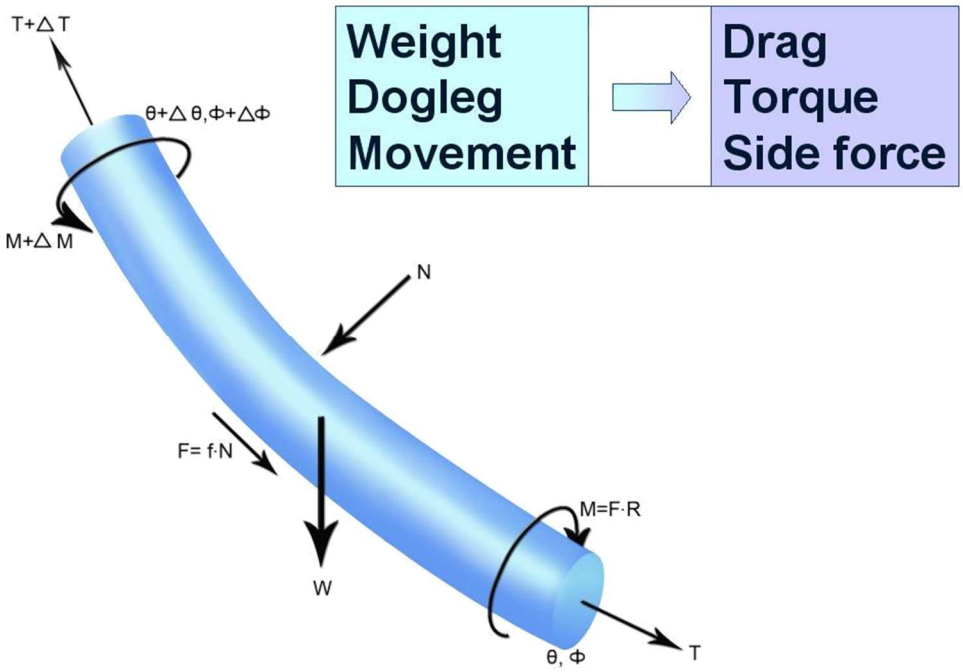

Figure 5: Forces acting on drill pipe at curved well section (Gefei, 2015)

Typical drilling operations use steel drilling pipe which require a large amount of force to bend leading to increase friction along the wellbore and increased frictional torque when rotating the drillstring. The second source of increased frictional resistance in horizontal wells is due to the pipe laying on the low side of the wellbore in the horizontal section. While drilling vertically the pipe makes limited contact with the wellbore, however, in the horizontal section the full length of the pipe rests on the wellbore with the pipe imparting friction load to the wellbore equal to the weight of the pipe times the friction coefficient between pipe and wellbore (Mirhaj, et al., 2010). Further exacerbating this issue is the tendency of cuttings generated during drilling to settle in the annular region between the drill pipe and wellbore in the horizontal well section. This settling can further increase the friction by partially surrounding the lower side of the drill pipe which can lead the pipe becoming embedded in cuttings. However, these problems can be mitigated by vibrating the drill string which lowers the frictional coefficient experienced between the drill pipe and wellbore by approximately 25% (Skyles, et al., 2012).

Excessive friction can lead to any number of problems including drill string buckling, stick slipping of the bit face, inability to hold tool face, pipe sticking during tripping in or out of hole and weight stacking (Skyles et al., 2012). Drill string buckling occurs when the WOB needed to drill exceeds the ability of the drill string to resist collapse against the sides of the well bore and can occur in a sinusoidal (due to vertical forces) or helical (due to torque) fashion as shown in Fig. 6.

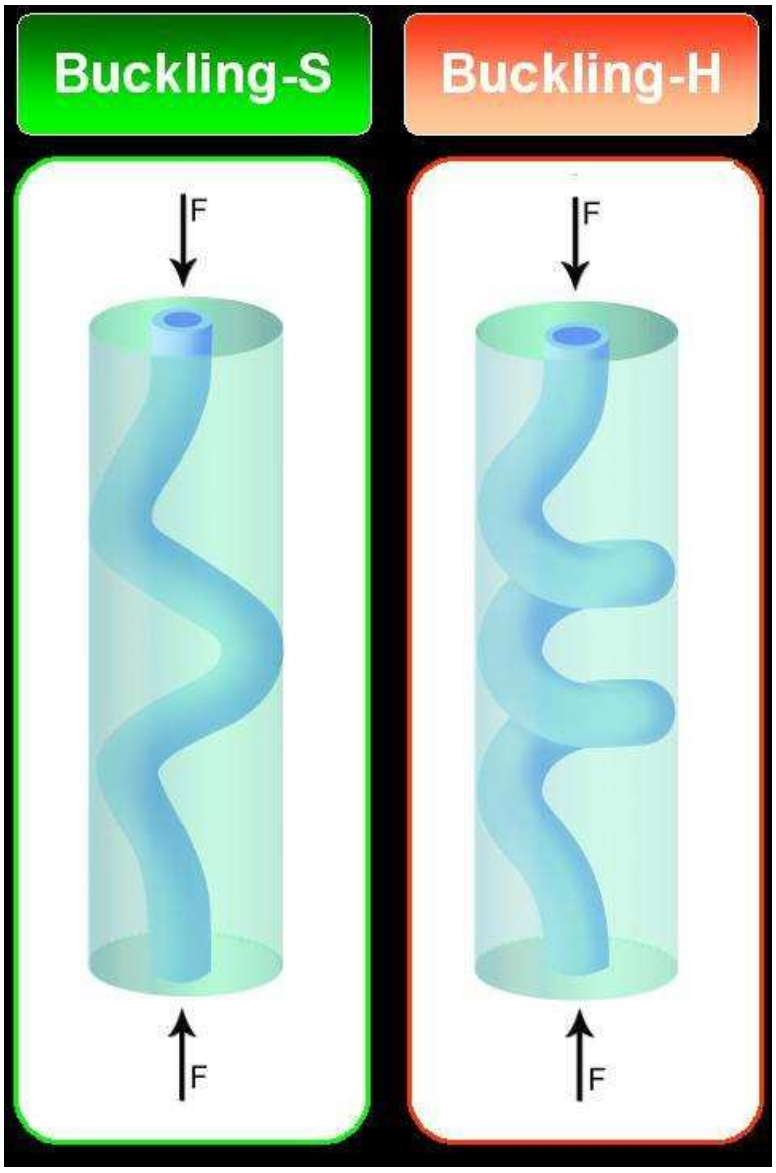

Figure 6: Sinusoidal buckling (left) and helical buckling (right) of drill pipe due to excessive friction (Gefei, 2015)

Once collapsed the contact area of the drill string along he wellbore is increase leading to more overall frictional force which can damaged the wellbore and limits the WOB that can be applied to drill. Excessive friction during rotational drilling in which the drillstring is rotated while drilling can cause a condition known as “stick slippage” in which there is micro-stickage between the bottom hole assembly (BHA) and wellbore while rotating followed by a sudden lurch as the rotation unsticks when the friction exceeds a critical value (Fear, et al., 1997). This process can occur several times a second and can lead to premature wear and total failure of large diameter PDC bits. Even if the bit is not damaged by this stick slipping it still makes controlling the tool face much more difficult and can lead to lower ROP. Weight stacking can also occur when the cumulative friction along the entire drill string exceeds the applied WOB and results in little or no ROP during drilling (Fear, et al., 1997). In order to combat these problems a friction reducer called “AG-itator” that was operated by using a rotor-stator configuration to periodically open and closed a path for the drilling fluid flow was installed and tested along a drill string to cause vibrations (Fear, et al., 1997). During testing in Texas, a 30% decrease in the WOB needed to optimize the ROP and a 12.5% increase in the ROP on average along the section drilled compared to historical data from offset wells was recorded (Fear, et al., 1997).

2.2 Bit Cleaning and Hydraulics

In cases where the friction doesn’t constrain the drilling ROP the ability to efficiently clean the cuttings away from the bit face often does. With poor cleaning the cuttings generated by the bit aren’t removed quickly or completely enough to avoid being reground. This regrinding contributes both to lower ROP as well as faster wearing out of the bit. There have been numerous studies regarding how to achieve optimal bit cleaning efficiency, however, with traditional PDC drill bits there is only so much improvement to be made. Some of the first methods for optimizing bit cleaning were pioneered in 1960 which found that regardless of which term (hydraulic horsepower, impact force or jet velocity) was maximized the ROP was increased and that the

ROP was positively related to the pressure drop across the bit (Kendall & Goins, 1960). This improvement in cleaning efficiency as a function of the product of jet velocity and flowrate was independently confirmed in later research with the note that the primary deterrent to achieving maximum drilling rates was the inability of the drilling system to remove rock cuttings efficiently enough to prevent interference with the drilling action (Mclean & Cheatham, 1964) (Yarbrough, 1964). Building on this knowledge, a full size jet-bit was tested in an attempt to further understand both bit cleaning and a phenomenon known as "chip hold down" in which the cutting chips generated are held to the well bottom by the pressure of the drilling fluid column (Sutko, 1973). By closing one or two bit nozzles the chip removal force was increased and it was stated that this should assist in the cleaning of the bore and improve the ROP (Sutko, 1973). Furthermore, the removal force acting on a chip is predominantly due to inertia and friction caused by fluid viscosity plays a minor role (Sutko, 1973). In theory, a pulsating bit like the DBB could overcome the initial inertia required to move a chip more effectively than a constant pressure jet drill bit since the initial pressure wave created when a fluid path is opened in the DBB has greater force than a bit with the nozzles constantly open due to the back pressure developed when the fluid paths are closed. Experimentally, the maximum impact pressure occurs when the pressure drop across the bit is between 45-80% of the overall pump pressure (Smalling & Key, 1979). By closing one or more nozzles periodically the pressure drop across the bit can be artificially elevated to this range more easily possibly leading to both greater ROP and enhanced bit cleaning. Another significant advancement in bit cleaning knowledge was the relationship between fluid turbulence and chip removal (Wells, 1989). By embedding chips of a known size and shape in a synthetic hole bottom held in place by hydrostatic pressure and then removing them with the jet action of a single impinging jet and measuring the jet turbulence it was possible to predict the necessary conditions for chip removal (Wells, 1989). The results of such testing indicate that chip hold-down forces can be overcome by the turbulent action of the jet nozzle and that maximum turbulence leads to the most efficient cleaning (Wells, 1989). Turbulence is

described as a time variance in a flow field; by pulsing the drilling fluid and changing the drilling fluid path more turbulent flow could be achieved by the DBB than a traditional PDC drill bit. A final hydraulic concern during drilling is avoiding a condition known as pump-off where the pressure beneath the bit due to the jets forces the bit off the bottom of the wellbore. The most common ways to avoid pump-off are to decrease the area of the bit face and to lower the average pressure of the jets (Hudgins, 1975). Typically, the bit diameter is fixed so this only leaves the average pressure as a possible way to avoid pump-off. By fluctuating the pressure of the jets a greater maximum impact force can be obtained which is proven to improve the cleaning efficiency while the average pressure would remain constant as is the case with the performance of the DBB. This could lead to a greater ability to clean the bit and lift cuttings away while avoiding pump-off.

2.3 Confinement Rock Strengthening

Detailed study into the fracture mechanics during drilling has generated models that predict the work or energy required to crush a specified volume of rock. In general, an increase in the hardness or ductility of rock decreases the drillability of the rock. However, the properties of rock can change due to extreme heat and pressure, both of which are present in deep wells. Deep underground the pressure exerted by the earth above is so great that it compacts the rock, reducing pore volume and increasing the hardness of the rock. There is a triaxial or near triaxial state of stress on undisturbed rock underground and so the pressurization of pore liquid within the rock is the driving force behind the rock strengthening because only the triaxial component of stress will contribute to this strengthening effect (Garnier & Van Lingen, 1959) (Maji, 2011). In other words, the increase in strength resulting from depth is caused only by the difference between wellbore pressure and in-situ pore pressure (Warren & Smith, 1985). At the bottom of a borehole the state of stress is different than the undrilled state as the component oriented along the drill string direction is now due to the fluid pressure of the mud column as well as the jets on

the bit (Prasad, 2009) instead of the vertical column of earth. The component of pressure induced hardening due to the fluid jet could possibly be reduced by flow interruption which would lower the pressure under the bit in the interrupted zone for a short period. If it were possible to reduce one component direction of stress the hardness of the rock would decrease proportionally despite other two component directions remaining the same. This effect could possibly occur under the DBB where part of the flow was interrupted as this interruption would depressurize one area of the bit face. This depressurization could lower component of stress experienced by the rock in the well bore direction thus lowering the pore fluid pressure and in turn the hardness of the rock. This confinement hardening effect is most pronounced in Mancos shale (six times increase in hardness at depth) which represents a large fraction of the formations drilled in North America (Kolle, 1996). A second factor impeding the ROP during drilling is the tendency for shales to increase in ductility and the increase in percentage of ductile versus brittle fractures as the confining pressure increases (Block & Jin, 2009). Regardless of whether the hardness increases in shales, the increased ductility consumes more energy for a given volume of cuttings leading to a decrease in ROP (Warren, 1985). By studying the micro mechanical behavior of a variety of crystalline materials, including crystalline rocks, it was demonstrated that this "transition from brittle to ductile failure occurs when the applied strain rate is sufficiently low to allow creep deformation to relax stress concentrations at flaw tips or when the confinement is sufficient to prevent frictional sliding along flaws" (Renshaw, et al., 2011) lending further credence to the need to reduce confining pressures on the borehole bottom. By reducing the confining pressure exerted on the formations being drilled both the hardness and ductility increases can be minimized.

2.4 Vibration

While the type of vibrational mechanisms similar to the DBB are a relatively new invention the study of the effect of vibration on drilling efficiency has been active for much longer. In the past, traditionally vibration in drilling was restricted to the use of vibratory drills which were often

used for coring operations and the created vibrations were of low amplitude and very high frequency (on the order of KHz). However, research from this are can still be used to guide design principals for tools like the DBB as there is some crossover. ROP increases with increase in vibration amplitude; this increase is approximately linear until close to the peak ROP, where the rate of increase in ROP is noticeably higher (Li, et al., 2010). There also appears to be an optimal value of vibration amplitude at a given WOB and rotary speed, with the ROP decreasing an increase in vibration amplitude beyond this optimal level(Li, et al., 2010). The greatest effect of vibration occurs when the vibrational frequency of the bit approaches the natural or resonant frequency of the substrate (Lianggang, et al., 2014) (Wei, et al., 2013). When this condition is met the drilling speed of sonic vibratory drills is five times that of traditional rotary drills (Lianggang, et al., 2014). ROP has been found to increase linearly with rotary speed when no vibration is applied on the rock and approximately exponentially when harmonic vibration is applied (Wei, et al., 2013). Furthermore, ROP more than doubled when drilling at the resonant frequency of the rock in sandstone is a recent study and the fracture mechanism induced by vibrations could possibly increase wellbore stability (Wei, et al., 2013). However, the resonant frequency of sandstones is from 1.58-2.56 kHz (Wei. et al., 2013) and for less porous rocks, the frequency has been recorded as high as 37 kHz (Li, et al., 2010). While this is orders of magnitude greater than either the DBB or similar designs can generate the vibrational improvements were demonstrated all the way down to the range of these designs (<100 Hz), albeit with reduced efficiency.

2.5 Similar Designs

Over the past two decades a variety of downhole vibrational and pulsation generating tools have been created and tested in the field with almost universal success. The gains in ROP and bit life measured during field tests and operation have been substantial and inducing vibration either along the drill string or at the bit has become an accepted performance enhancing mechanism.

However, detailed knowledge of the exact mechanisms responsible for these performance enhancements is shaky at best and this limited knowledge has hindered the optimization of vibration and pulsation generation. Because drilling rates decrease continuously with depth in fluid-filled boreholes due to the confining effect of borehole pressure depressurization of the rock being drilled has been studied as a means of increasing the ROP during drilling (Kolle, 2000). Impulsive depressurization of the borehole can overcome the confining pressure and induce effective tensile stress at the cutting face, increasing the drillability of the rock (Kolle, 2000). To achieve this depressurization a design using a flow interruption mechanism mounted above the bit was tested. A valve was periodically opened and closed leading to short periods of flow through the bit (Kolle, 2000). This design created very short-lived pressure drops (2-3 msec) creating a fairly stable high maximum pressure as shown in Fig. 7 below.

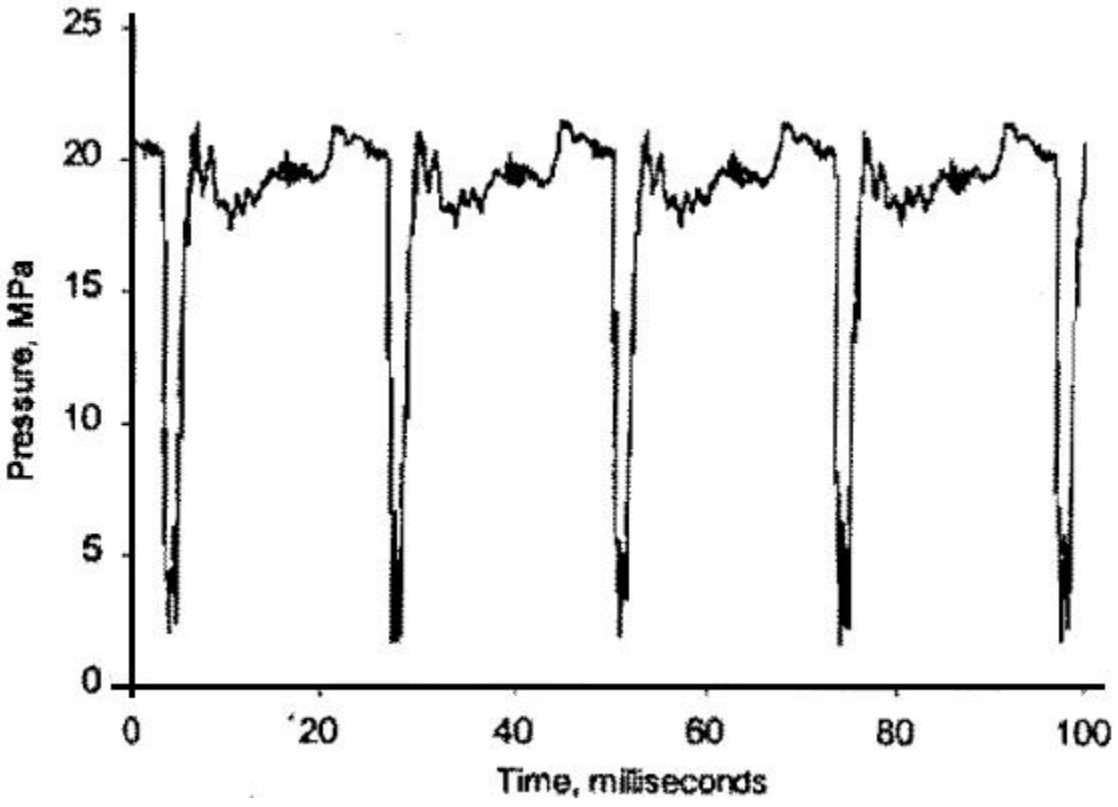

Figure 7: Pressure vs. Time of flow interrupter (Kolle, 2000)

During field testing the section drilled with the flow interrupting mechanism outperformed the historical ROP of offset wells which drew industry attention to the possibility of achieving further performance improvements through the creation of improved pulsation mechanisms (Kolle, 2000).

Due to the intense heat and stress during the drilling of deep wells it is beneficial to have as few moving parts as possible since they tend to wear out leading to breakage which usually requires the drilling operational to halt and trip the entire length of drill string out of a well to repair the broken component. With this in mind another design which also generated pressure pulses was created by modifying bit nozzles that were operated without the need for a mechanical valve or moving components (Gensheng, et al., 2011). Several different configurations of organ-pipe and Helmholtz style self-resonating chamber nozzles were tested as shown in Fig. 8.

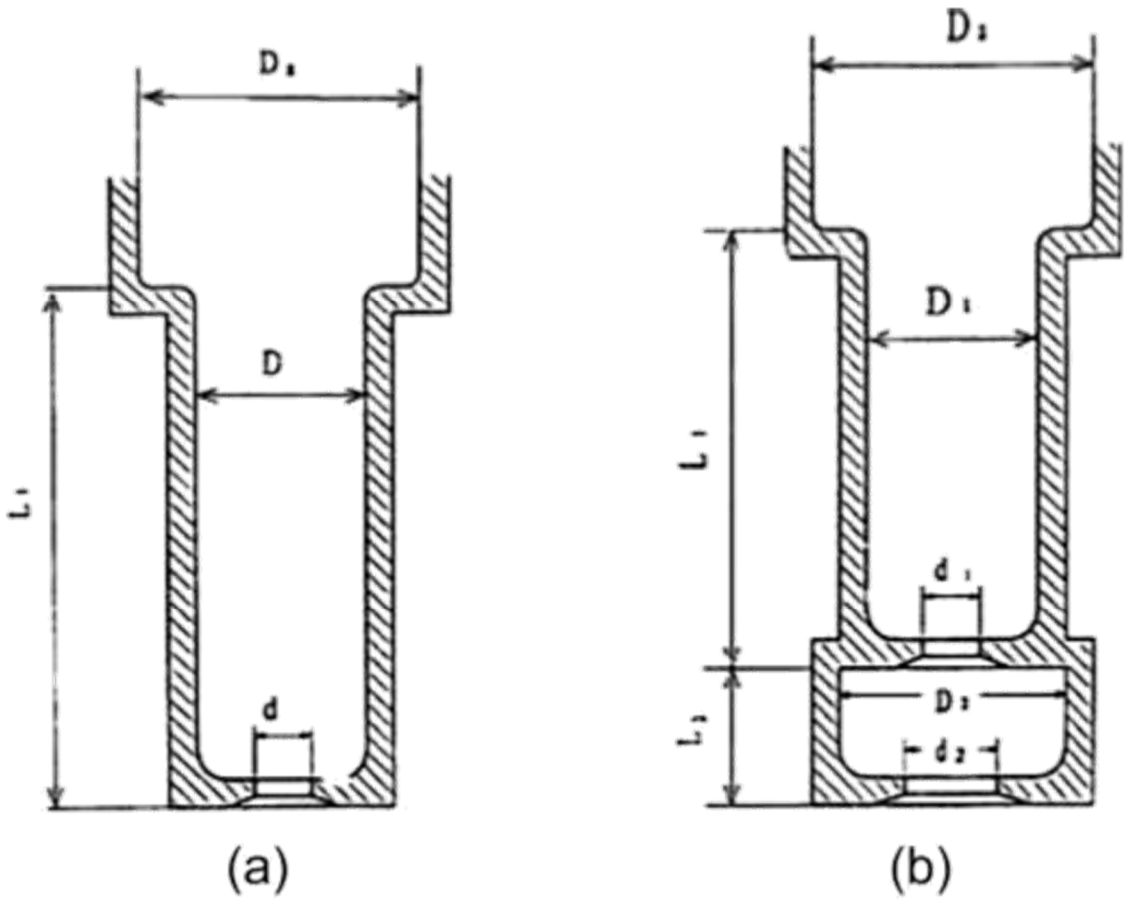

Figure 8: Self-resonating cavitating jet nozzle design schematic (Gensheng, et al., 2011).

By adjusting the outlet and resonance chamber dimensions self-resonating pulsations through the bit nozzles were created. The nozzles were installed in tricone style bits and tested in over 500 wells in China in a large field study. Under the same conditions, compared to the conventional cone shaped nozzles, self-resonating cavitating nozzles enhanced average rates of penetration by 31.2%, improved bit total penetrations by 29.1% and enhanced rock erosion efficiency 1–2 times (Gensheng, et al., 2011).

Another pulsation tool was created called the Drilling Agitator Tool (DAT) which used a rotor stator mud motor to spin a plate with one large hole over a stationary plate with a matching hole shown in Fig. 9 (Barton, et al., 2011). Each revolution would open and then close the hole one time changing the flow area and creating a pulse of pressure when the hole was closed at a

pulsing frequency of 10-20 Hz. The design was tested in over 100 wells and recorded a 31.6% average increase in bit footage, over 50% increase in ROP for many wells and a 30% average increase in bit life.

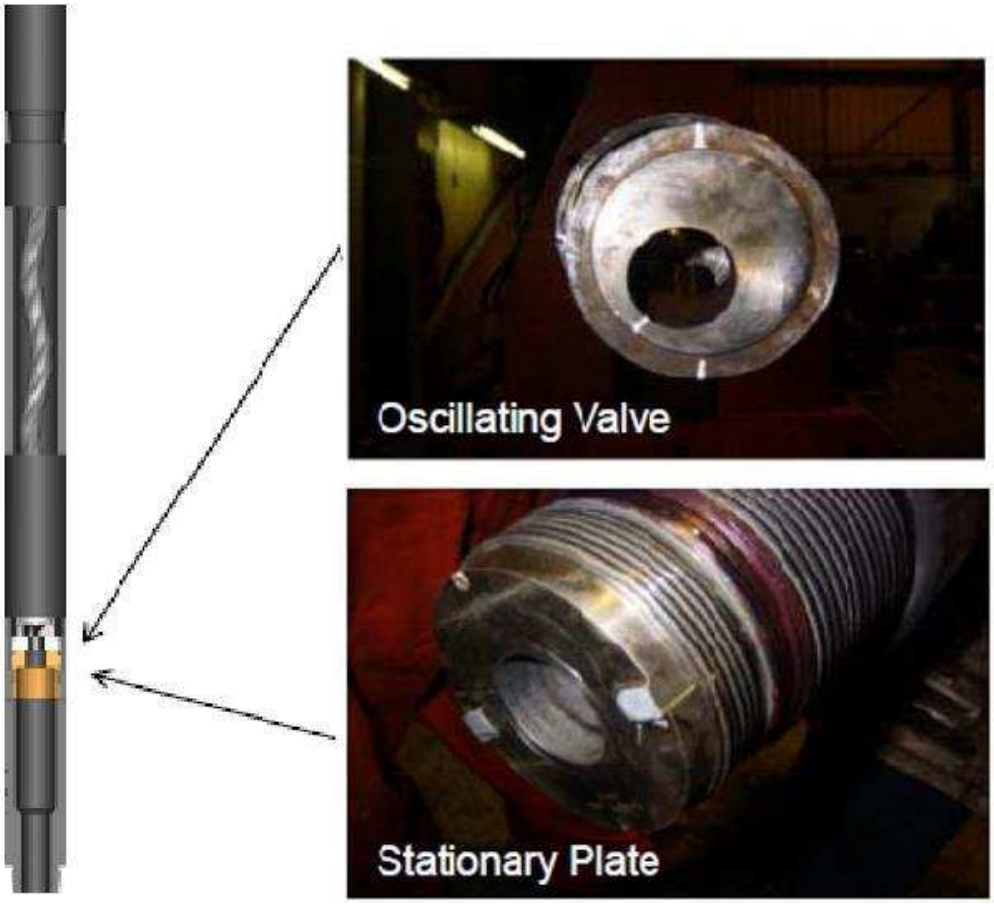

Figure 9: "Drilling Agitator Tool" (DAT) pulsation design (Barton, et al., 2011).

Two years later a similar design emerged which also created pressure pulsation due to a rotating interrupting mechanism (Cui, et al., 2013). However, instead of using a single rotating hole the interruption mechanism was situated above a cavitation chamber so that the pulsations would be magnified as shown in Fig. 10.

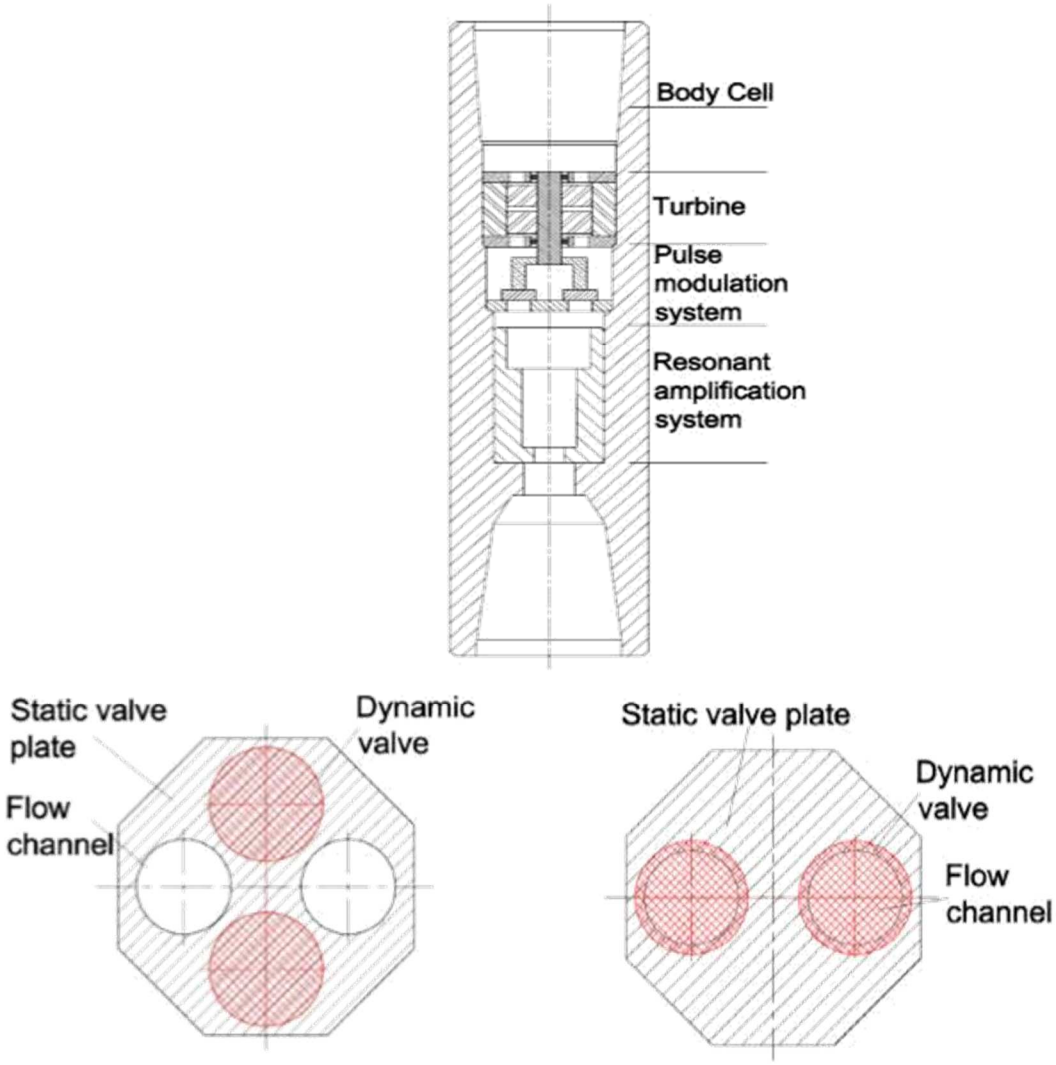

Figure 10: Pulsation tool with turbine (Cui, et al., 2013)

A variation on the existing pulsation mechanisms that employed a spinning impeller in the flow within the BHA was tested as well and is shown in Fig. 11 (Fu, et Al., 2012). The pulsation was increased due to cavitation behind the impeller blades creating localized impact pressure of 8.6-124 times the pressure of the free jet as the cavitation volumes collapsed. The pressure in the drillstring was measured near the surface of the well and pressure fluctuation amplitudes of 250-350 psi at around 10 Hz recorded (Fu, et Al., 2012). The design was tested in ultra-deep wells (5000m-7000m) and a 10.1-31.5% increase in ROP and average of 29.1% increase bit footage life recorded.

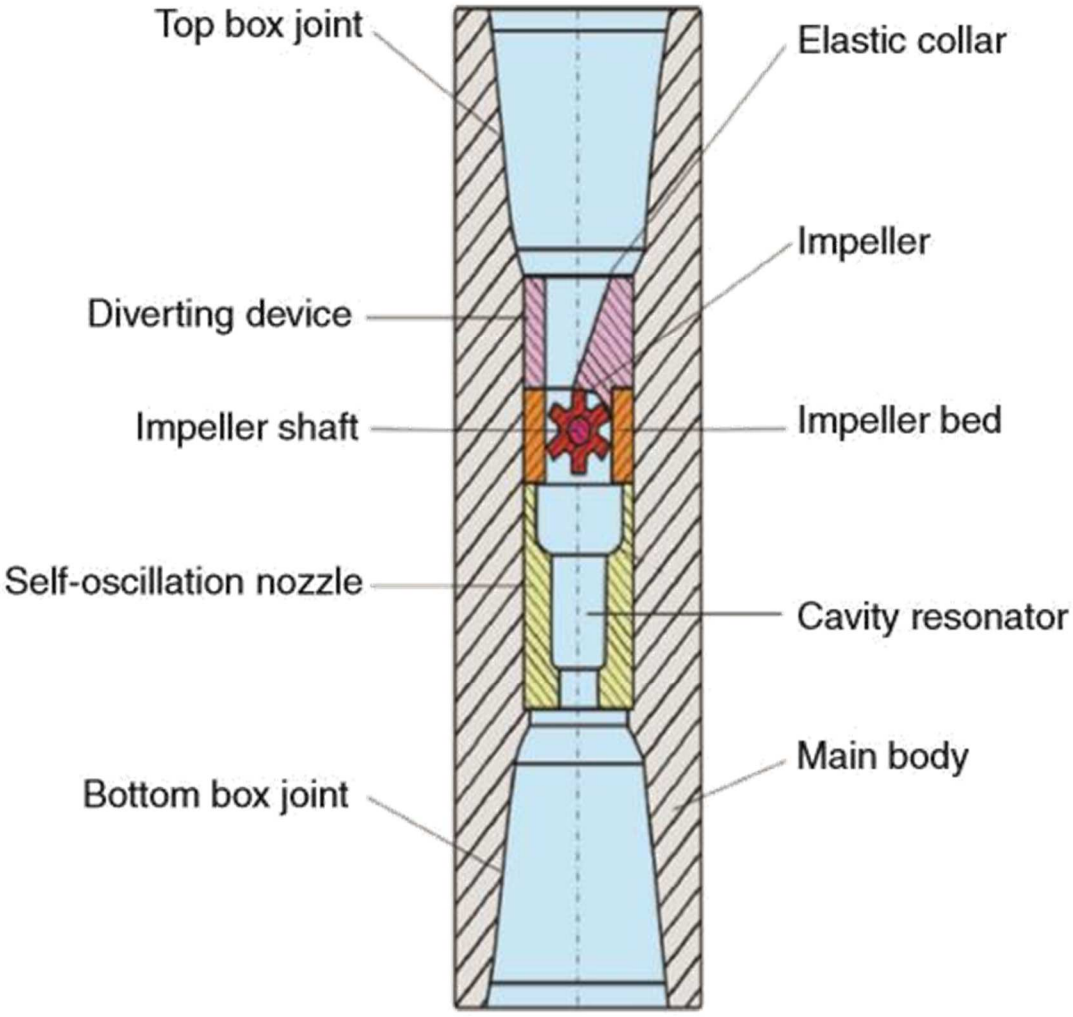

Figure 11: Cavitating impeller pulsation design (Fu, et al., 2012)

It is important to note that cavitation alone, whether at the nozzle or above the bit, has been shown to not always lead to improved cutting efficiency or an improved ROP. Instead, the drilling system must be compliant to the vibrations produced by the tool in order to intensify the natural displacement vibration of the compliant element (Badapour, 2014).

The last design variation that has been developed acts similarly to a jackhammer in that the axial vibrations are generated by the extension and contraction of the bit. These vibrations displaced the bit head between 3-11mm at 8-11 Hz during testing and led to a 114% and 212% increase in ROP compared to offset well data during the first and second tests, respectively (Herrington &

Barton, 2013). In the second test 74% more distance was covered by the bit compared to the offset well historical performance; data regarding footage for the first test was not available. A view of the fluid hammer assembly is shown in Fig. 12.

Figure 12: Fluid hammer design (Herrington & Barton, 2013)

CHAPTER III

EXPERIMENTAL METHODOLOGY AND TESTING

In order to analyze the response of the bit to various design changes and flowrates it was important to understand which measurements were most important to guide the design of the experimental set up and data acquisition system. The DBB's primary function is the modulation of the pressure in the bit. The rate and pressure of the fluid discharge from the nozzles is both a function of the instantaneous orientation of the interrupter plate as well as the internal pressure of the bit. The orientation of the interrupter plate could be deduced from video footage of testing by noting which jets were active and the relative magnitude of the jets to one another. However, recording the pressure posed a major problem- where and how to record the pressure. In previous literature the pressure had been recorded at the nozzle jets, at the surface of the drill string, and inside the pulsation mechanism chambers with testing occurring both above and below ground. Since recording accurate pressure thousands of feet underground would be both costly and difficult and since there was deemed no advantage to be gained from measuring underground during an actual drilling operation as opposed testing was conducted above ground and the pressure measured at the midway point along the pressure chamber wall. A test matrix consisting of four interrupter plate designs and three different flowrates was constructed in order to cover a wide range of conditions and enable the creation of a more robust physical model based on analytical calculations and backed by experimental pressure data.

3.1 Previous Testing

The DBB had been previously tested in 2013 in a limited series of experiments measuring the pressure as a function of time and the flowrate of the pump providing the fluid pressure. The pump was connected to the bit via flexible tubing and the pressure was recorded with a pressure transducer while the pump was tested at 120, 200, 250 and 300 GPM. The bit was strapped down to a wooden pallet as shown in Fig. 13.

Figure 13: Previous DBB testing set up in 2013

At this point the only interrupter plate in existence was a two-hole interrupter plate design. A limited amount of analysis was conducted which calculated the pressure drop across various choke points along the DBB in an attempt to predict the amount of flow powering the rotor stator which spun the interrupter plate as well as plotting the pressure as a function of time in order to

get a rough estimate of the pulsation amplitude and average pressure. The goal of this testing was to determine how to better control the amount of flow to the rotor stator. Analysis and testing was concluded before a definitive solution was reached.

3.2 Overview of Recent Testing

The DBB was tested at the University of Missouri Science and Technology Rock Science Lab in Rolla, MO in the summer of 2015. A Halliburton HT-400 series 250 kW (335 HP) triplex pump provided fluid pressure to the bit from a 37.8 cubic meter (10,000 gallon) holding tank (pool) as shown in the testing schematic in Fig. 14.

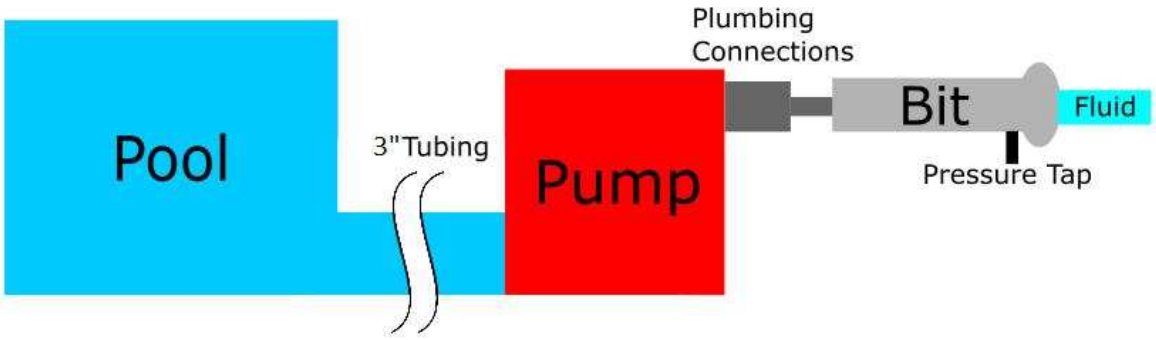

Figure 14: Testing schematic

The water holding tank was connected to the pump with a flexible 76 mm (3 in) diameter, 6 m long hose. The volumetric flowrate was measured by multiplying the drop in water level within the holding tank by the tanks cross-sectional area and dividing by the duration of each test (100 seconds). The bit was connected to the pump by 50 mm (2 inch) iron piping that was approximately 1 m long with two right angle joints and was strapped down to a semi-rigid support structure so that it would remain in place and discharge water over a field without anything blocking the exit stream as shown in Fig. 15.

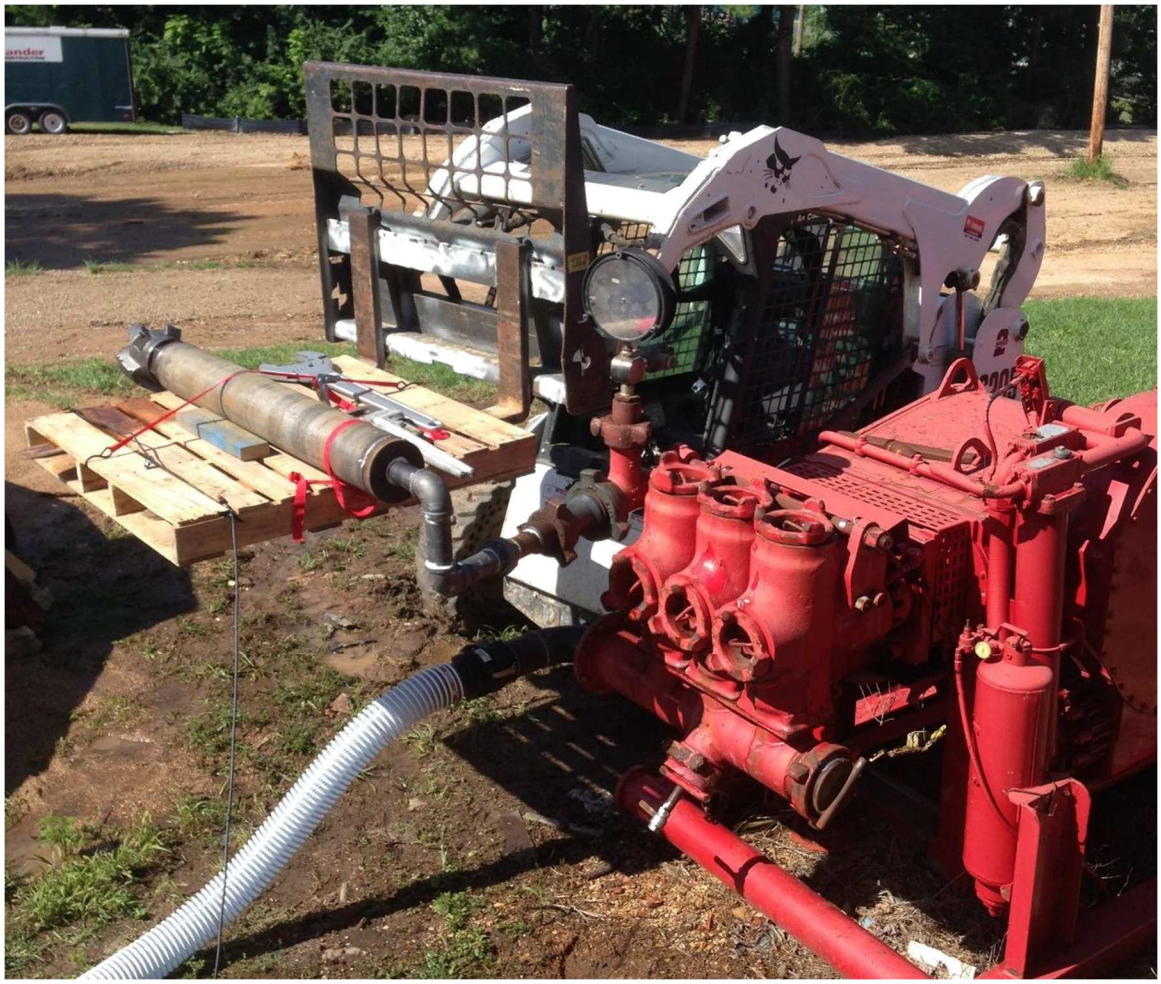

Figure 15: Experimental test setup

3.3 Plumbing Connections

A 6.35 mm (¼ in) ID, 380 mm (15 in) long hydraulic hose was threaded into a 6.35 mm NPT tapped hole drilled in the body of the bit and connected to a 0-20 MPa (0-3000 PSI) pressure transducer (PX309-3KGI, Omega) to measure the internal bit pressure fluctuations of the drilling fluid before it was expelled through the nozzles, as shown in Fig. 16 and 17. The location of the tapped hole for pressure measurement was chosen based on in its position relative to the middle of the pressure amplification chamber. The hydraulic hose was used instead of a direct connection to the bit to isolate the transducer from the bit vibrations and enable more accurate measurements.

By recording the pressure close to the interrupter plate the closest approximation of the pressure through the nozzles could be obtained.

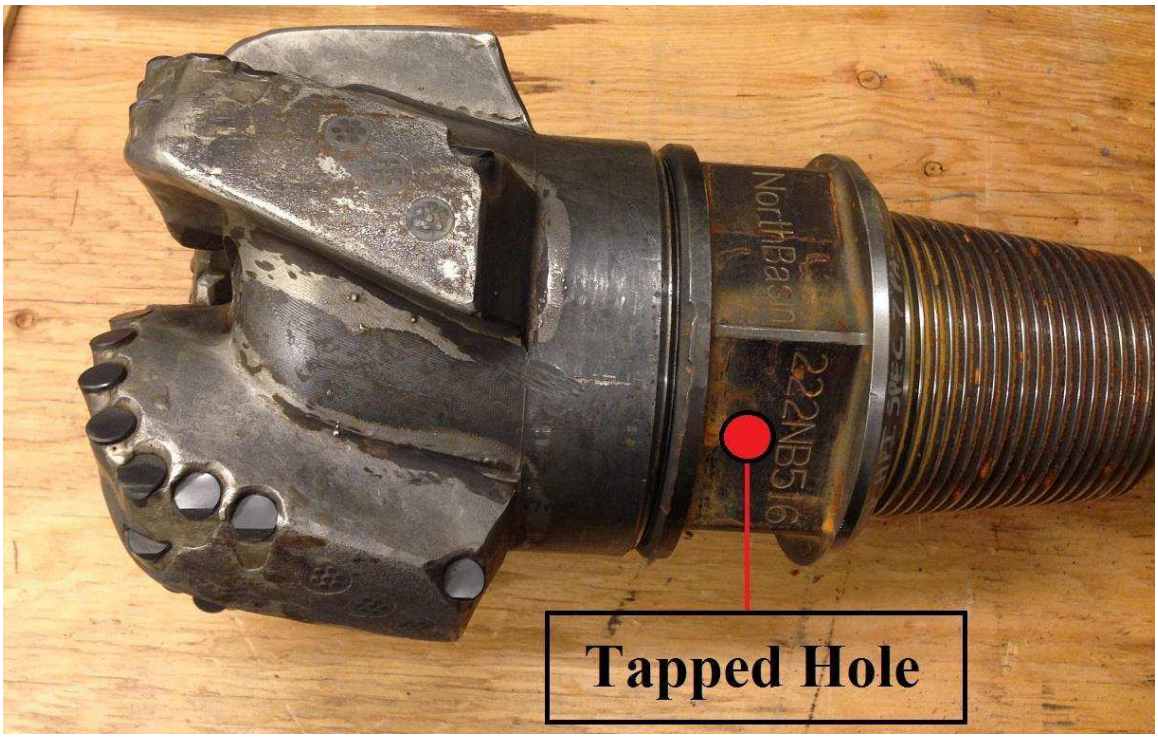

Figure 16: Tapped hole pressure measurement location

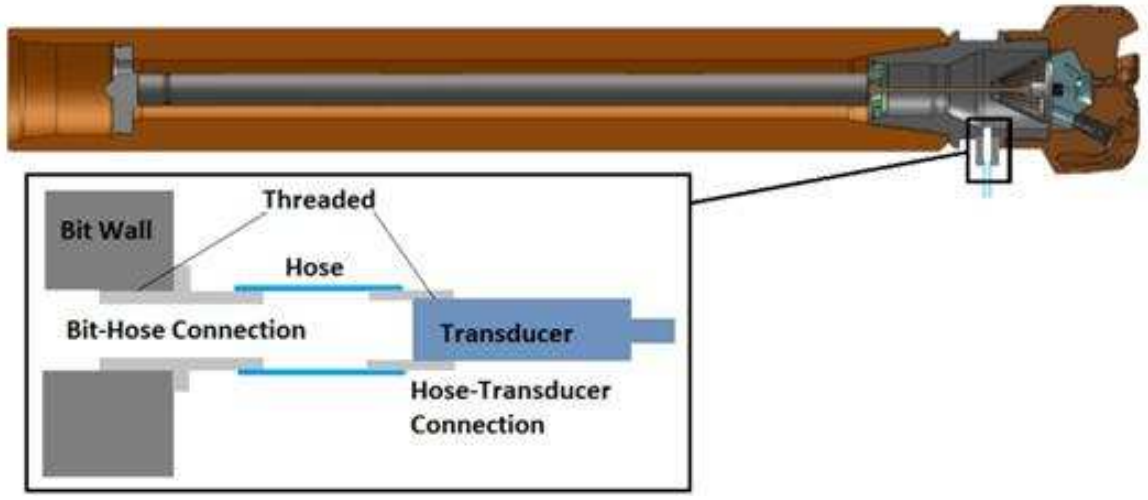

Figure 17: Pressure measurement plumbing connections

3.4 Electrical Circuit Design

The electrical circuit used to convert the output current from the pressure transducer to a recorded voltage is shown in Fig. 18 and was composed of a 6 m BNC cable, which transmit the pressure transducer current across a 560 Ohm resistor. The output voltage measured across this resistor and the input voltage supplied by a 24 V power supply was routed to a NI USB-6218 BNC data acquisition instrument connected to a Lenovo Ideapad laptop computer running a Labview VI, which recorded the output and input voltages.

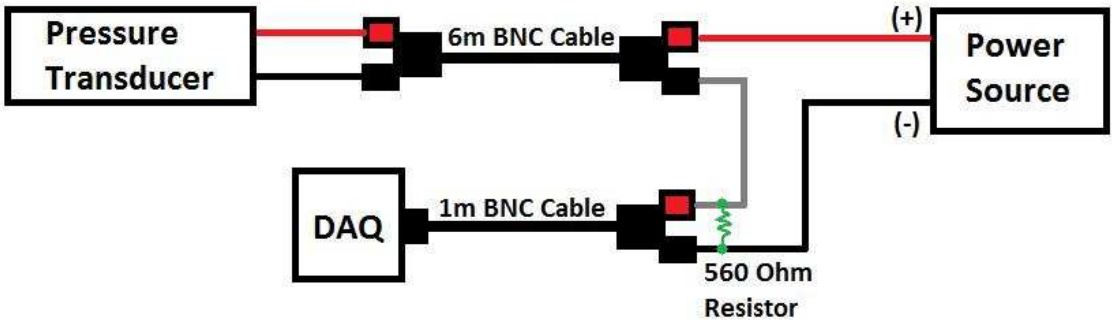

Figure 18: Electrical circuit schematic

By measuring the voltage across a 560 Ohm resistor the 0-12 volt range of the DAQ instrument was maximized while still enabling the maximum pressure of 3000 PSI to be recorded. The calculations to arrive at these values are shown below in Eq. 1 using Ohm's Law (Encyclopædia Britannica, 2014) where is the voltage measured (Voltas), is the current from the pressure transducer (Amps) and is the resistance of the resistor (Ohms).

$$V = I * R \tag{1}$$

The output range of the pressure transducer used was 4-20 mA with a pressure of 0 PSI registering a 4mA output and a pressure of 3000 PSI registering a 20 mA output. The sensitivity of this transducer would then be 187.5 PSI/mA. Therefore, by using a 560 ohm resistor the maximum pressure output from the transducer of 20 mA would correspond to a voltage output of 11.2 volts and a pressure of 3000 PSI.

3.5 Data Acquisition

Testing was conducted by ramping up the pump to the desired RPM and then recording 100 seconds of data at a sampling rate of 1000 Hz once a stable pump output had been achieved. Prior to data collection the exact pulsation frequency of the DBB was unknown so a cautious estimate of the maximum possible frequency of was 100 Hz was used to calculate the Nyquist rate of sampling which is the minimum sample frequency capable of measuring a given signal without aliasing (Dataq.com, 2013). For a maximum frequency of 100 Hz this Nyquist rate would be 200 Hz. The sampling rate used during testing of 1000 Hz was five times the minimum rate necessary as this rate was well within the computing power of the system and would allow for greater resolution of spectral content during data processing.

3.6 Interrupter Plate Design

Four interrupter plates were tested with each design being created to maximize different individual aspects of the pressure fluctuation in order to gather data on a wide range of input conditions. The plates will hereby be referred to in an abbreviated form with the first number standing for the number of holes, the second letter representing the word “hole” and the third letter (if applicable) representing any additional information regarding the plate design. The two hole plate (2H) was machined out of steel with hole diameters equal to the outside nozzle diameters in the bit and hole spacing such that the holes opened and closed nozzles simultaneously with a 2/5 rotational spacing between the hole centers. This plate was intended to be used as a baseline to compare the performance of the other designs against and existing for the 2013 bit testing. The edges of the plate had a chamfer and a carbide friction disk in the center of the plate which was slightly raised as shown in Fig. 20. The three hole plate (3H) was machined out of 6061 aluminum and had three holes of the equal diameter to the 2H plate spaced such that one hole was offset from the other two so that when the two matched holes would close the offset

hole would open. The goal of this design was to increase the frequency of pressure pulsation as well as study the effect of pulses of two different magnitudes, which would be created by two holes opening at once followed by only one hole opening shown in Fig. 19. The two hole long (2HL) was also made of 6061 aluminum and had two holes with hole profiles that were elongated along a circular arc a distance of one hole radius with slightly over 2/5 rotational spacing between hole centers such that the front edges of the holes were offset by one half a hole radius. This plate was intended to maximize bit cleaning as the longer hole openings would allow for more flow before being closed resulting in a higher flowrate at any given pressure and is shown in Fig. 22. The one hole (1H) was cut with a water jet from brass and designed to minimize plate sticking due to galling and debris build up and to test the effect of minimizing nozzle restriction and maximizing the high pressure/low pressure variation across each side of the bit face. It had one hole that was extended so that the hole ran ½ the length of the plate diameter along a circular arc, which would lead the nozzles on one side of the bit being open while the other half of the bit would be closed shown in Fig. 21. A summary of the four plate designs is shown in Table 1. A bottom view of the 3H plate is not shown because the central friction pad was removed and installed in the 2HL plate which is why there is a hole in the center of the disk. When installed the middle of the plate would look and function similarly to the 2HL plate shown.

Name	Holes	Materials
1H	1 Elongated	Brass body, steel center disk
2HL	2 Elongated	Aluminum body, steel center disk
3H	3 Circular, offset	Aluminum body, steel center disk
2H	2 Circular	Steel body, carbide center disk

Table 1: Interrupter plate information

Figure 19: 3H plate top view

Figure 20: 2H plate top view (above) and bottom view (below)

Figure 21: 1H plate top view (above) and bottom view (below)

Figure 22: 2HL plate top view (above) and bottom view (below)

3.7 Testing Conditions

The initial test matrix was composed of testing 3 different flow interrupter plates at a "low", "medium" and "high" pump RPM, where each speed represented approximately 1/3, 2/3 and full pump RPMs, respectively, for a total of 9 test conditions shown in Table 2. However, this matrix was expanded to include repeat testing of each plate to check repeatability of recorded data. The actual test data used for analysis is shown in Table 3. Some of the planned tests were not recorded as it was apparent some of the plates would only spin at the maximum pump RPM so the lower speed tests were not recorded when this was verified. The testing was conducted over the course 8/12/15 to 8/13/15 in Rolla, Missouri and the weather conditions were fairly stable at between 24-28 degrees Celsius and 1020-1023 hPa barometric pressure (conditions from wunderground.com).

		Flowrate		
		Q1	Q2	Q3
Rotor Plate	2HL	P1	P2	P3
	1H	P1	P2	P3
	2HL	P1	P2	P3
	3H	P1	P2	P3
		Pressure		

Table 2: Initial test matrix

File Name	Plate Type	Pump Speed	Flowrate, (GPM)	Date/Time
O L	2H	Low	111	8/12/2015 15:07
O L 2	2H	Low	122	8/12/2015 15:20
O M	2H	Medium	155	8/12/2015 16:15
O M 2	2H	Medium	200	8/12/2015 16:18
O H	2H	High	333	8/12/2015 13:03
O H 2	2H	High	388	8/12/2015 16:09
1 M	1H	Medium	402	8/13/2015 9:48
1 H	1H	High	498	8/13/2015 9:44
1 H 2	1H	High	505	8/13/2015 10:07
2 L	2HL	Low	138	8/12/2015 15:07
2 H	2HL	High	427	8/12/2015 15:15
2 H 2	2HL	High	445	8/13/2015 9:58
3 H	3H	High	444	8/12/2015 15:43
3 H	3H	High	436	8/12/2015 15:48

Table 3: Testing summary and conditions

3.8 Testing Observations

The testing was approached from a high level with several very different plate geometries, materials and flowrates in order to allow for a much broader scope of investigation on the effect of design and operating conditions on pulsation characteristics. A side effect of this was that much of the test matrix resulted in data that only invalidated certain designs, materials or operating conditions. Simple visual analysis of the tests indicated that the two aluminum plates (2HL, 3H) may have suffered from a degradation of pulsation consistency over the course of each test due to debris getting stuck under and along the sides of the interrupter plate resulting in galling and plate sticking. This was investigated by taking the DBB apart between each test and taking the interrupter plate out. Several times the plate would become somewhat wedged into its slot and be difficulty to remove due to chunks of small sand-like debris between the sides and bottom the plate and the slot it rotated in which is shown in Fig 23.

Figure 23: Slot for interrupter plate showing signs of gauging

The pump used to power the bit had rust and debris in the piston cylinders due to age that was the main cause of the debris induced sticking and a pump used in the field would likely not contain near as much debris. These sticking was minimized with the addition of lubrication on the interrupter plate, but such a solution would not be feasible in the field where the DBB could not be frequently taken out of the well hole for maintenance. The plate made of steel (2H) was the only design that utilized a carbide on carbide spinning disk contact compared to a steel on carbide contact used in the other three designs. This resulted in very low friction and high plate rotation speed, which appeared to open and closed the fluid paths so quickly that only a minimal amount of fluid was able to pass through the outer nozzles shown in Fig. 24, where the red lines represent the jet from the central (always open) nozzles and the black lines the very small weak jets from the nozzles being interrupted.

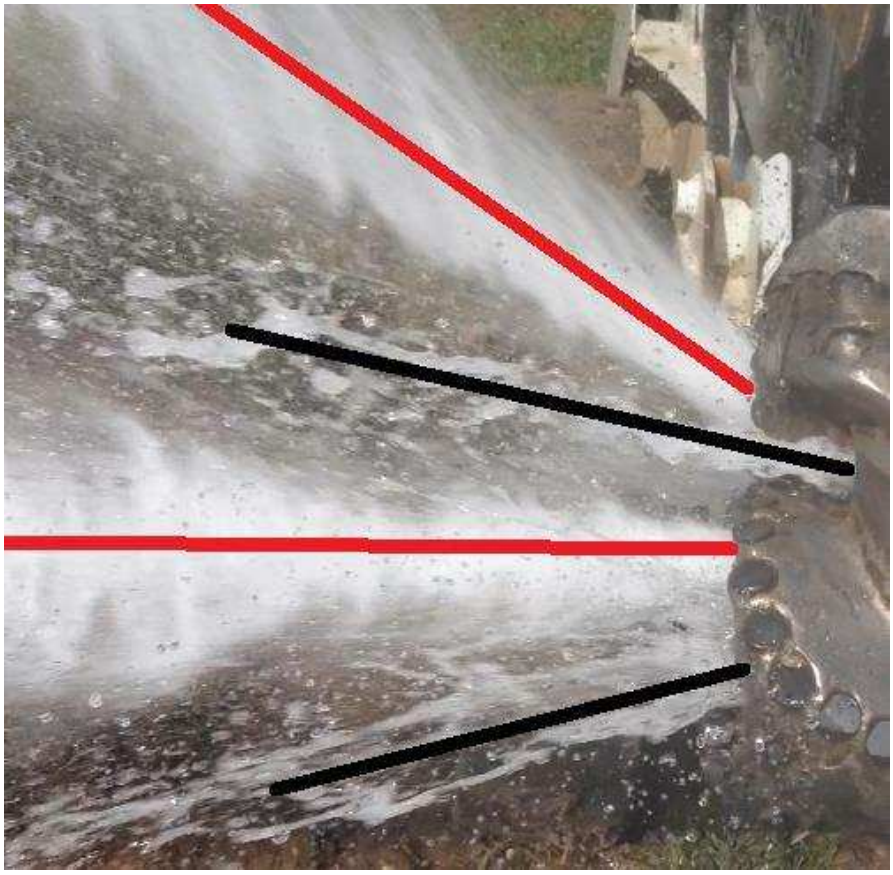

Figure 24: 2H plate testing jet comparison

Furthermore, at pump RPM's much below the maximum capability of the pump the flow rate and pressure created was too low to overcome the internal friction of the mud motor which resulted in the plate not spinning at all. A mud motor with a lower spinning pressure threshold could eliminate this problem in future testing. For the high pump RPM tests the average pressures ranged from 711 to 1470 PSI with peaks up to 1738 PSI which expelled fluid over a hundred feet from the bit as shown in Fig 25.

Figure 25: 2HL plate test side view (above) and downrange view (below)

CHAPTER IV

DATA ANALYSIS

4.1 Data Filtering

It was clear during testing that the pump surges due to the plunging action of each piston was causing an unwanted pulsing effect in the fluid not due to the bit alone. Therefore, before the data could be analyzed it first had to be filtered to remove the unwanted noise due to the pump. The triplex pump used was not fitted with a pulsation dampener so due to the piston action of the pump the dominant signal component in each test was consistently around 10 Hz at full pump output. In order to remove this unwanted frequency content a technique known as spectral subtraction was used. The basic theory of spectral subtraction is that by separating a signal into its discrete component frequencies and respective magnitudes any discrete component frequency can be subtracted from the original signal. This is helpful because once a signal has been broken into discrete spectral components a good approximation of the original signal can be rebuilt using these discrete spectral components through the use of an inverse Fourier transform (S. Boll, 2003). By subtracting all spectral components over a cut-off frequency a good approximation of the signal without the pump frequency can be obtained (R. L. Geiger, 1985).

The first step of this process was to use a fast Fourier transform (FFT) to discretize the input signal frequency components. A fast Fourier transform was used because it reduced the number

of computations needed for N points from 2^2 to $2 \log$, where log is the base-2 logarithm (Weisstein, 2014). This was done using a coding program called MATLAB which had built in function for both FFT and inverse FFT's (IFFT). An example of the spectral content of a test of the 2HL plate is shown in Fig 26.

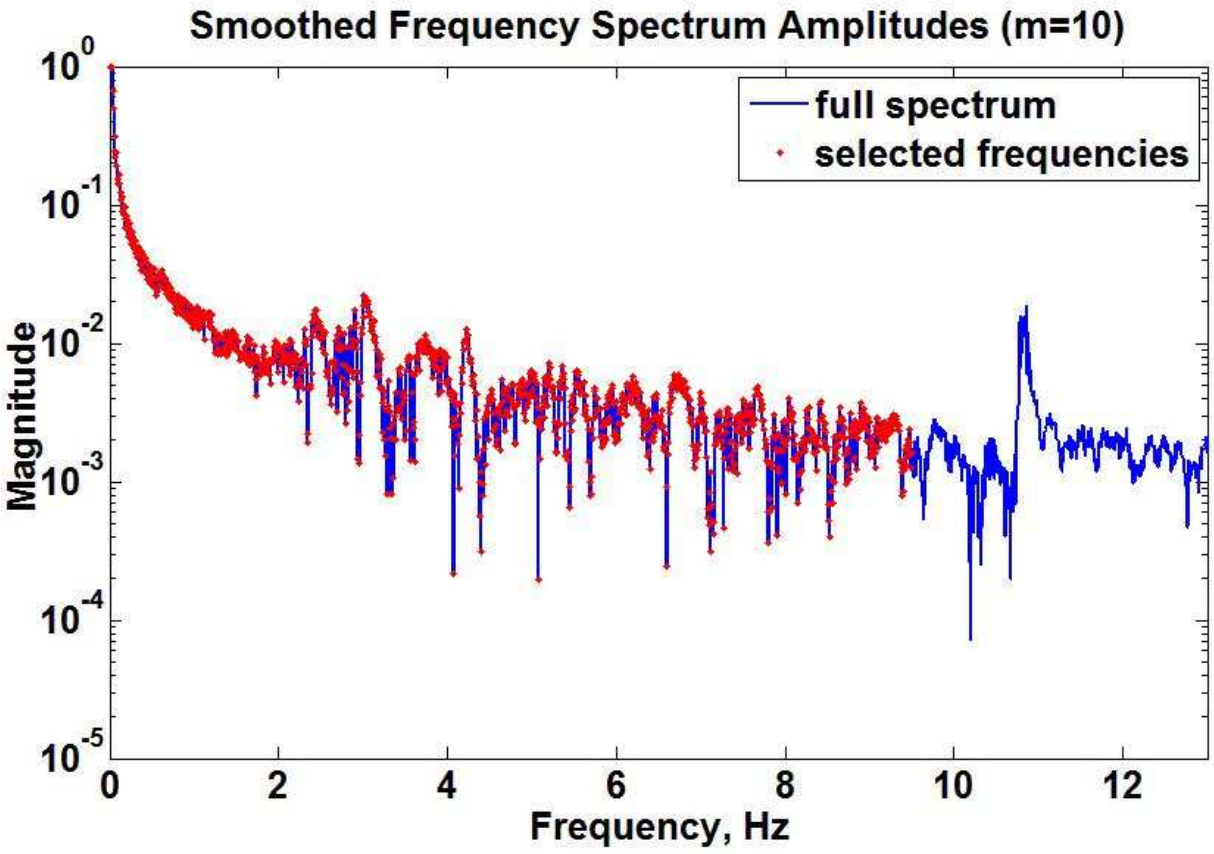

Figure 26: Frequency spectrum for 2HL plate plot

The user manual for the pump was referenced to calculate the expected pump pulsation frequency to ensure that the ~10 Hz was in fact due to the pump to avoid filtering out any more content than necessary. The bulk of the spectral content due to the interrupter plates was between 1-7 Hz which was below the pump frequency and thus was below the filtering cutoff frequency used of 9.5 Hz. Once the unwanted frequencies had been removed the remaining spectral data was run

through an IFFT to recreate the original signal only now without frequency components above 9.5 Hz. An example is shown in Fig. 27 below for the 2HL plate.

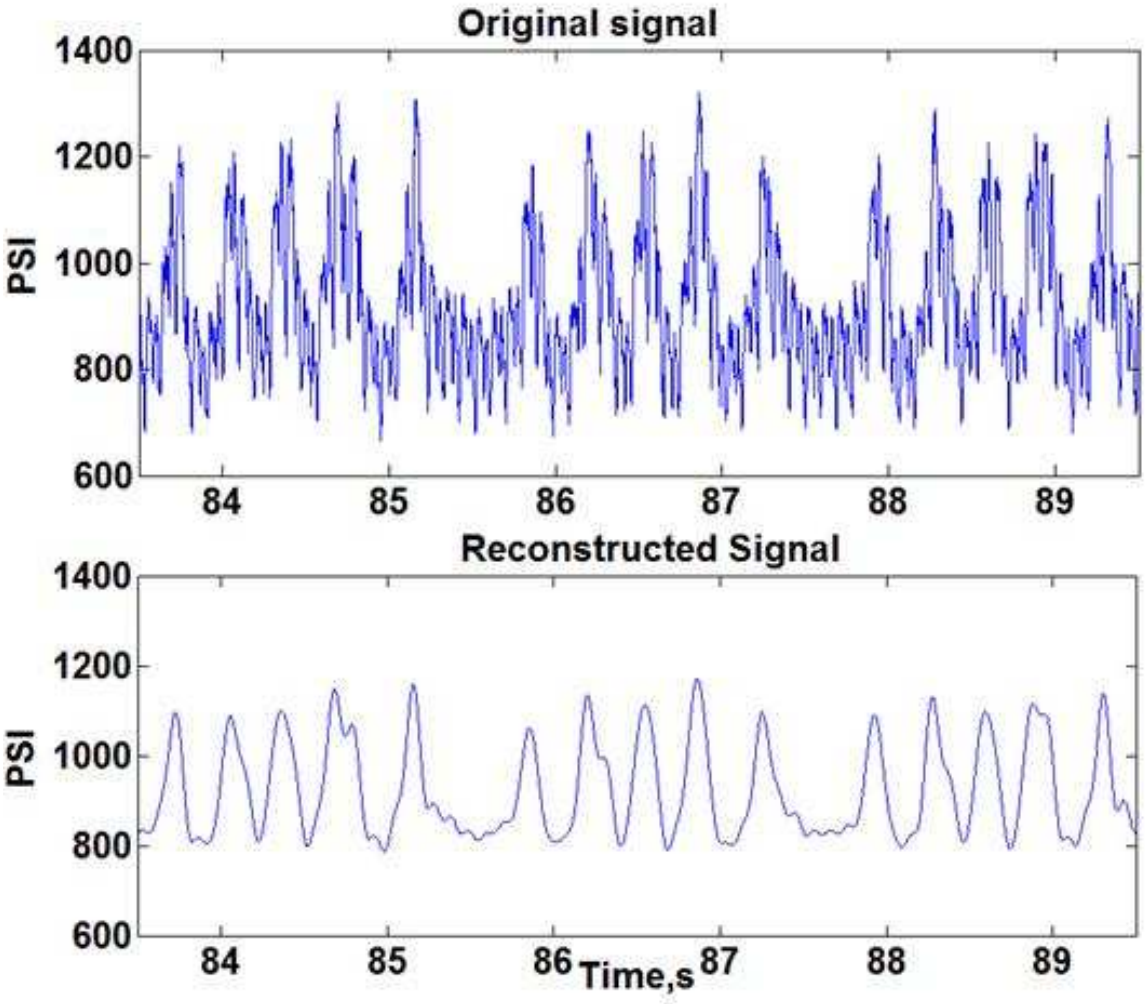

Figure 27: Original signal vs filtered signal plot for 2HL plate

A moving average of 10-15 data points was applied to the spectral data plots to allow for a better recognition of frequency peaks for plotting purpose. This allowed for a manual determination of the dominant frequency for each test which was used to determine the rotational frequency of the shaft powering the plate rotation and compared against video footage to verify pulsation frequency. Each rotation of the bit caused 5 pulses for each plate, other than the 3H plate since

the opening and closing of plate holes was in phase; one rotation of the 3H plate caused 10 pulsations since one hole was out of phase with the other two.

Upon comparison of this new testing data with the data obtained from the testing in 2013 shown in Fig. 28 it was clear that the pulsation performance measured was vastly different.

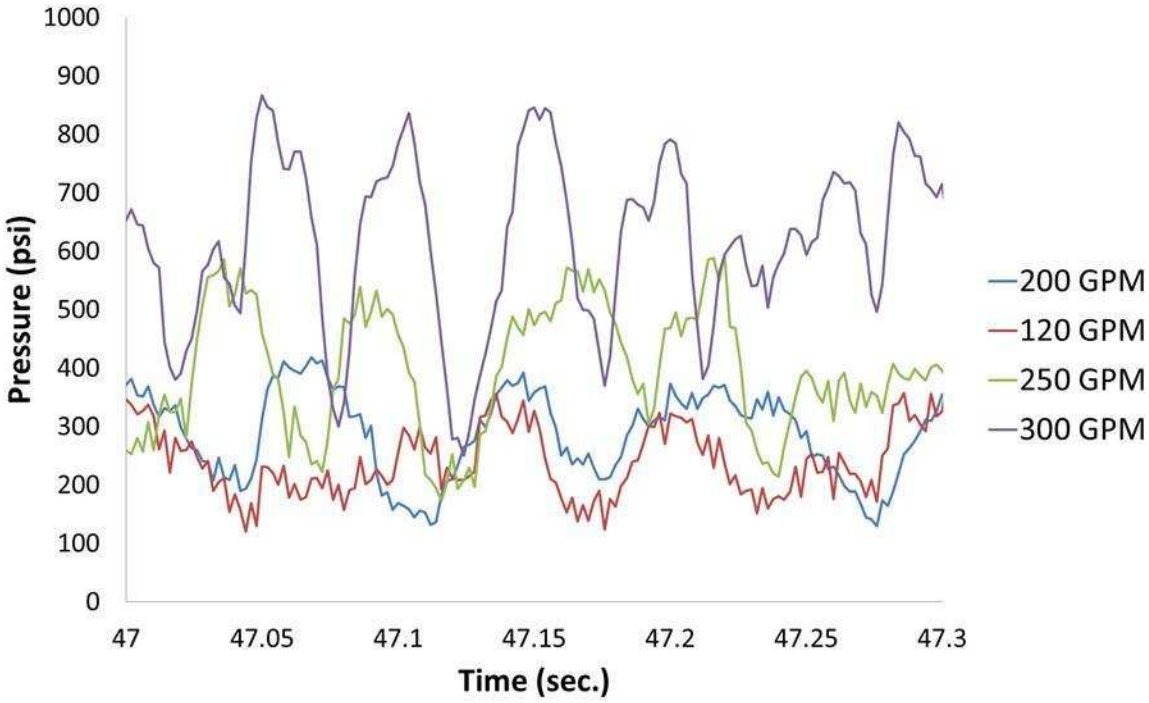

Figure 28: 2013 testing data plot at four flowrates

While the 2013 tested at flowrates less than this new round of testing the pulsation frequency and amplitude of pulsation as a fraction of average pressure was much higher for the 2013 testing. An attempt was made to rectify this difference by first extracting the dominant pulsation frequencies of the old test data in order to quantify the difference between the old and new test data. The pulsation frequencies are shown in tabular form in Table 4 and graphically in Fig. 29.

Summary of Dominant Frequencies							
120 GPM		200 GPM		250 GPM		300 GPM	
Hz	**Magnitude**	**Hz**	**Magnitude**	**Hz**	**Magnitude**	**Hz**	**Magnitude**
11.7	101	12.7	137	17.6	173	21.5	316
5.8	80	15.6	70	14.6	144	8.8	177
13.7	75	17.5	54	7.8	128	17.6	113
		6.8	54				

Table 4: 2013 testing pulsation frequency summary

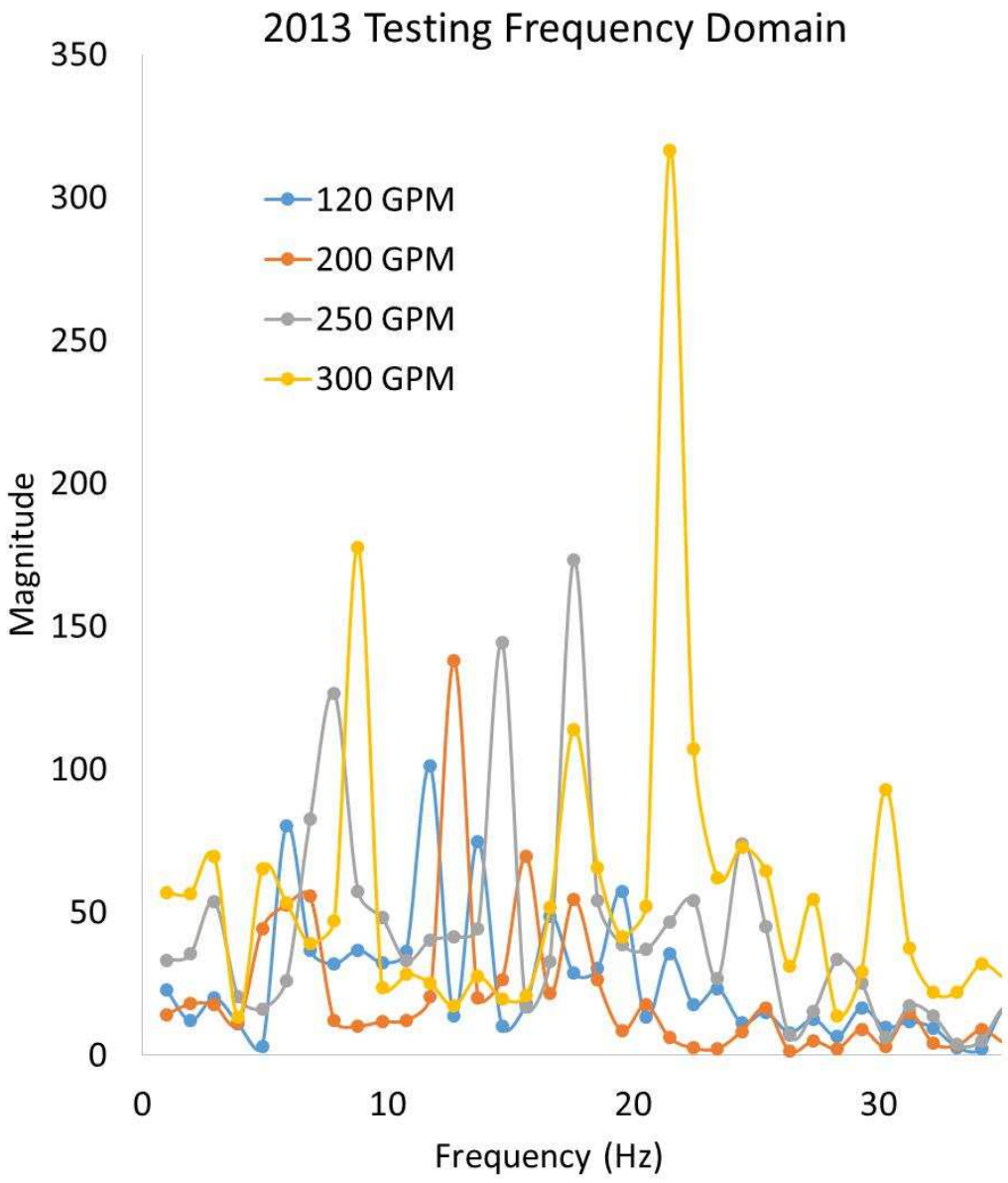

Figure 29: 2013 testing spectral content plot

The new tests with the 2H plate yielded an average dominant frequency of 3.3 Hz at a flowrate of 445 GPM while the 2013 testing recorded a frequency of 21.5 Hz at a lower flowrate of 300 GPM. Even more telling was the difference in the ratio of pressure pulsation amplitude to average pressure. The new testing yielded a ratio near zero while the 2013 testing measured a ratio of over one to one. Moreover when the 2H plate was tested in the more recent tests it spun too quickly to allow fluid to pass through the outside pulsing nozzles as discussed earlier which led to the near zero pulsation amplitude. Limited video footage of the testing during 2013 was obtained and compared to the videos from the recent tests and it was concluded that the pressure pulsation recorded during the 2013 testing was due almost exclusively to the pump. Because the pump surges were not isolated from the bit (as was the case in the recent testing as well) and because this pump frequency was not filtered out the data measured was simply a measurement of the pump pressure fluctuations due to the plunging action of the piston(s). Fig. 30 is provided below of the 2013 testing as a comparison to the recent test of the 2H plate shown earlier in Fig. 24. The low flow through the outer nozzles is shown in red and the inner (always open) nozzles are shown in black.

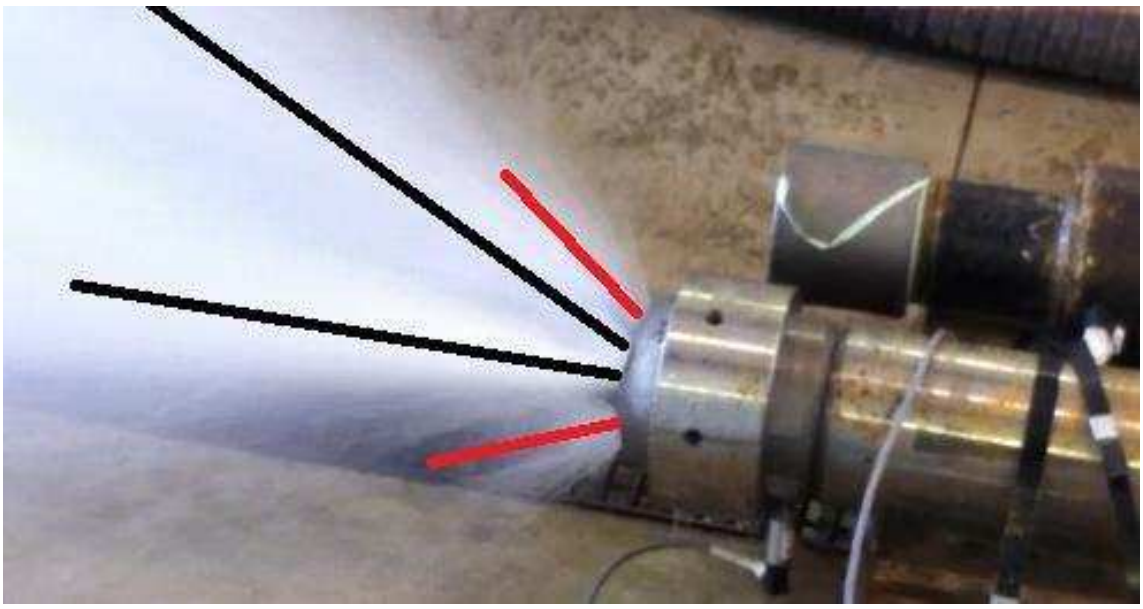

Figure 30: 2013 testing showing limited flow through outer nozzles (in red) vs. inner nozzles (black)

4.2 Interrupter Plate Performance

The filtered data for each of the four plates tested is shown in Fig. 31. Clearly the 2HL plate produced the largest pressure variations, however, they didn't always follow a smooth sinusoidal wave shape; instead, there was a second and sometimes a third smaller peak following many of the large initial peaks. There also appeared to be a less repeatable peak shape and pattern for this plate. This lack of consistency was also visually observed during testing and attributed to debris build up upon internal inspection. The other three plates (2H, 3H and 1H) did not create significant pressure pulsation at all. Due to the poor pulsation performance of the other three plates compared to the 2HL plate much of the analysis that followed focused on this plate design in an attempt to understand why it performed so much better and to quantify this performance increase. While the 3H plate did in fact create some sporadic pressure pulses they were highly erratic and this section of test data shown in Fig. 30 is of a period in between pulses. Due to the erratic nature of this plate it is possible that the filtering method may have been unable to accurately recreate the testing data since the pulses were not very repeatable due to significant plate sticking.

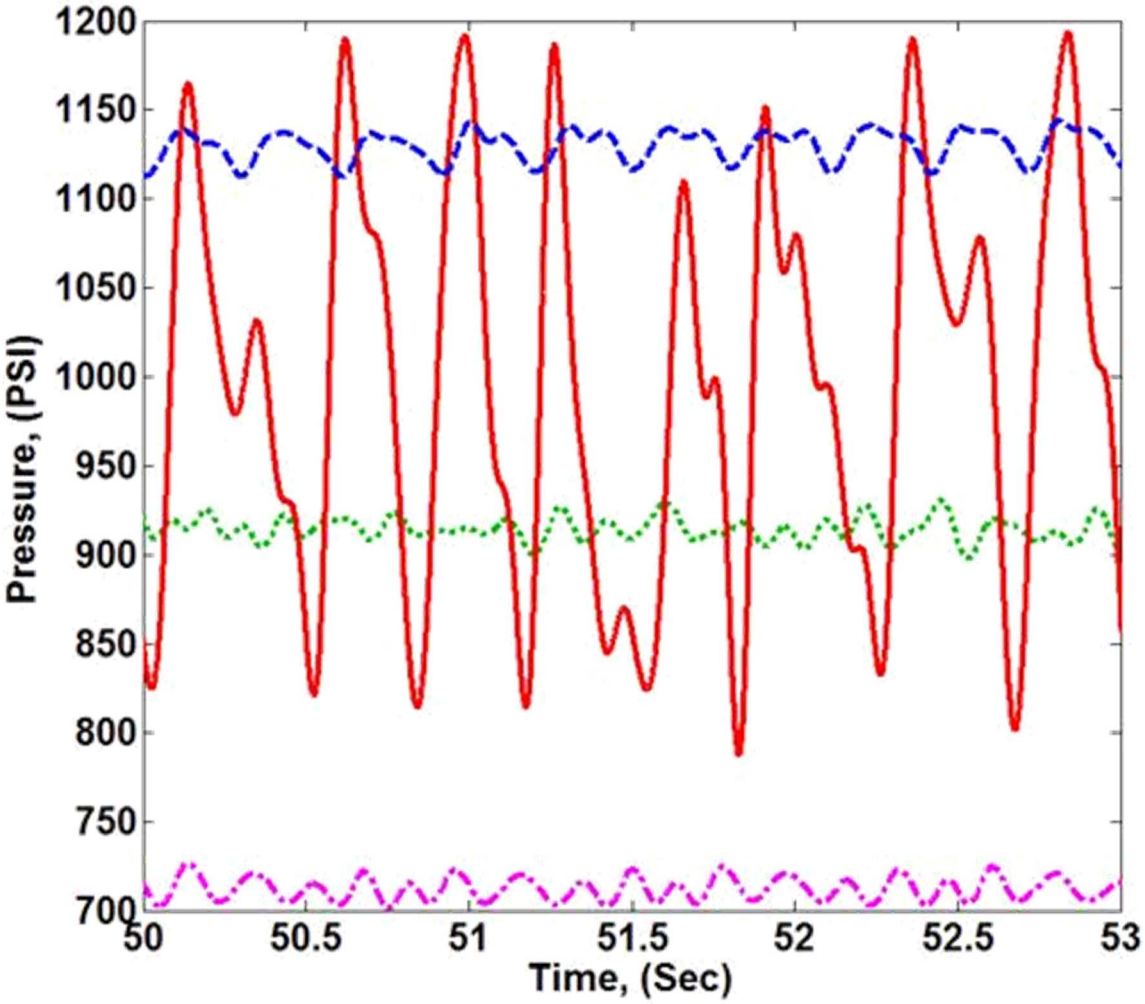

Figure 31: Filtered plate pressure comparison plot. Red=2HL, Blue=2H, Green=3H, Pink=1H.

There are several key observations about the 2HL plate performance obtained from both the spectral data as well as the pressure plots:

1. Repeatable variations of around 2 MPa (300 PSI) or 30% of the average pressure were obtained after filtering
2. The calculated average pressure was lower than the median pressure
3. The spectral content had many diffuse peaks instead of only one dominant one
4. The spectral peaks due the DBB were observed between 2-6 Hz (depending on if the 2nd smaller peaks are counted)
5. There was a sustained low pressure zone after each 5th peak

The magnitude and frequency of the pressure pulsations for the 2HL plate closely matched those obtained during testing in Li et el. (2005) which measured a maximum of 2 MPa (300 psi) pulsations at 10 Hz during the testing of a similar pulsation tool. There also appeared to be a long low pressure zone at the end of every fifth peak which would correspond to one full revolution of the flow interrupter plate. Within each set of 5 pressure spikes there were also some longer low pressure zones which could have indicated that there may have been a significant resistance to closing open fluid paths while the plate spun. The observation of low pressure zones was also reflected by the measurement of approximately 5% lower average pressure than median pressure. For a sinusoidal wave if the median is greater than the average (as was calculated) this indicates that the wave either has longer "troughs" than peaks which was observed in experimental data. If this was due to the resistance to closure of open fluid paths it could limit the pulsation frequency of further designs as water is nearly incompressible and the faster a plate spins the greater the shearing force that must be imparted to rotate the plate and close the fluid paths. Further limiting the frequency capability of this design is the inability of a significant amount of fluid to pass the interrupter plate when spinning at high speed as seen during testing of the 2H plate. Despite these possible frequency limitations many vibrational tools commercially available operate effectively at below 10 Hz. While there was likely a coupling effect between the pump frequency and DBB pulsation frequency often in the field there is no pressure spike dampener used during drilling so that the bit also experiences pressure pulsations downhole due to the pump. The amplitude and frequency of these pulsations are a function of many things including the pump type, model, output, length of drill pipe, fluid properties, pressure drop along drillstring, and drill bit and the effect of these pulses on vibrational tools deserves further study.

Video analysis of the testing showed that there might have been a reduction in the consistency of pulsation during some of the testing, which was attributed to a buildup of debris along the sides and bottom of the plates, particularly the aluminum plates. This was a concern for

further designs and was investigated by plotting the spectral content of the first third, middle third and last third of each test. By comparing the spectral content for each third of the test data any change as a function of time would be visible. This change would likely be due an increased plate rotational friction leading to a lower and less consistent pulsation frequency as the pump output and other variables were kept constant during each individual test. Using this methodology each test was examined and the aluminum plates (2H and 3H) were the only ones where significant variation in spectral content was observed during testing. An example of this change is shown in Fig. 33 for the 2HL plate where the red line represents the 1st third of testing, green the 2nd third and blue the last third.

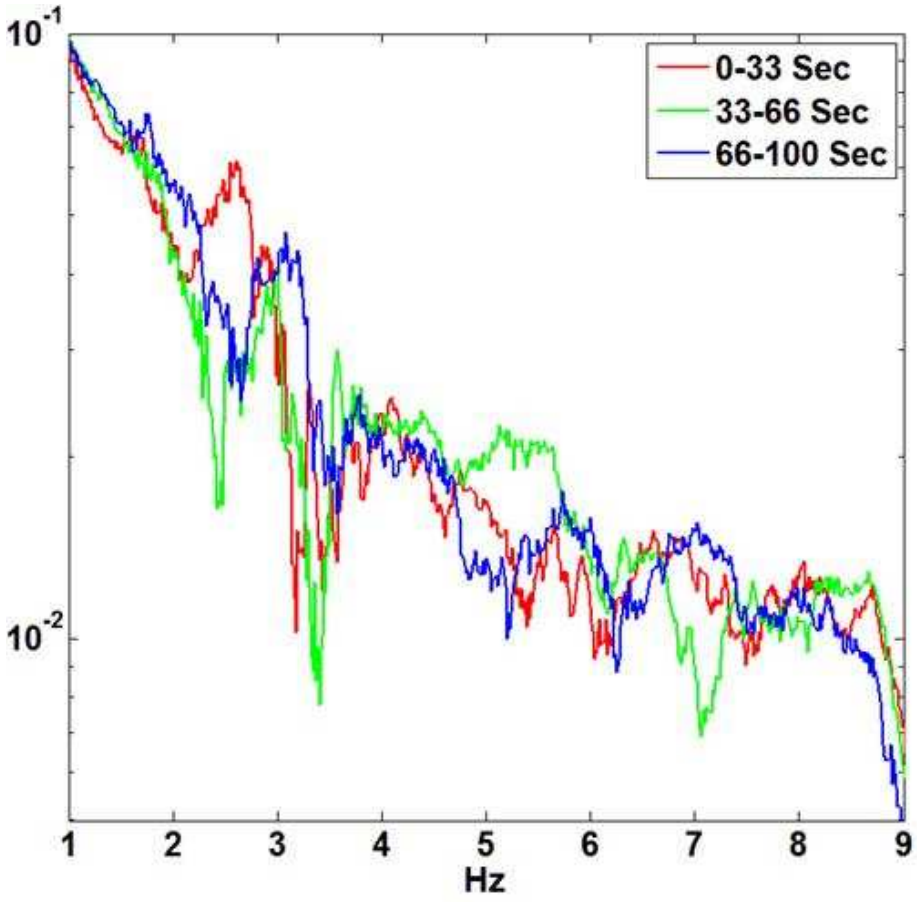

Figure 32: Spectral variance during 2HL testing plot

There was a clear shift in the frequency peak locations for the testing as indicated by Fig. 32, which depicts data from the second testing of the 2HL plate. The first frequency peak was approximately 3.1 Hz, which then dropped to approximately 2.7 Hz before returning to 3.1 Hz again. There was also variance in the magnitude from 4.7 to 6 Hz for the 33-66 second content further indicating something happened in the middle of this test to disrupt the pulsation frequency. However, Fig. 32 is one of the most dramatic examples of frequency variance during testing and a similar comparison of content across all tests did not generate any trends. The random nature of the variation in this test was likely due to debris in the holding tank such as sand, or rust in the pump or plumbing that sporadically broke free during testing and became stuck around the plate. Despite this change in frequency the average pressure for all the tests at the beginning middle and end of each tests had very little variation (less than 2%) validating the test results and methodology and indicating that the pump output remained constant during each individual test. In the future it might be possible to reduce this sensitivity to debris by using a mesh screen to block the passage of large debris to the plate. A summary of the measures of variance for each test is shown in Table 5 where the pressure drift term was calculated as the difference between the average pressure for the first 5% and last 5% of each test. This was used to check that the pump output remained constant during testing, which it did to within 1% of the average pressure for all tests.

File Name	Plate Type	Pump Speed	Pressure Drift, (psi)
O L	2H	Low	2.5
O L 2	2H	Low	-0.8
O M	2H	Medium	0.8
O M 2	2H	Medium	0.9
O H	2H	High	39.2
O H 2	2H	High	6.5
1 M	1H	Medium	3.7
1 H	1H	High	5.8
1 H 2	1H	High	2.4
2 L	2HL	Low	-0.2
2 H	2HL	High	5.2
2 H 2	2HL	High	11.3
3 H	3H	High	0.9
3 H	3H	High	0.9

Table 5: Pressure drift during each test

4.3 Interrupter Plate Design Effects

During testing it was clear that there were several competing design factors in pulsation performance. The overall pulsation efficiency was also strongly effected by plate material, friction pad material and buildup of debris around and under the plate.

The 2H plate with the carbide on carbide contact produced the highest rotational frequency. However, the holes opened and closed so quickly that there was negligible contribution from the outside pulsation nozzles and nearly all the flow was expelled through the two central nozzles which were always open. This led to a very high average pressure (10 MPa or 1500 psi) without substantial pulsation. This plate did not suffer from a drop off in rotational consistency or speed likely due to the chamfer around the edges of the plate which prevented debris from becoming lodged between the plate edge and the bit wall. The slight rise of the friction pad above the plate surface also minimized contact area and further decreased friction and debris lodging. The plate was made of steel as which could have also prevented sticking due to debris by crushing debris particles without galling or gauging of the plate occurring. This plate

was the clear best performer in terms of rotational consistency and an ability to withstand debris buildup. However, the pulsation power created was a small fraction of the overall fluid power and as a result this plate was largely unsuccessful.

The 3H plate was also unsuccessful due to a severe drop off in performance resulting from debris build-up and high spinning friction. After each 100 second test the bit was taken apart and the plate examined and there were deep galling marks across the underside of the plate shown in Fig. 33 indicating that the pressure exerted by the drilling fluid was warping the plate slightly so that the entire underside of the plate was in contact with the bit due to the lower stiffness of the aluminum compared to the steel plate (not shown) (Scari et al., 2014).

Figure 33: Interrupter plate gauging comparison. 2HL plate left, 1H plate right

This was undesirable for several reasons; (i) the increased contact could lead to a premature wear out of the plate if used in the field and (ii) debris in the drilling fluid, which would be normal for most drilling operations, could cause the plate to bind up requiring removal of the bit from the well to maintain it. These issues could possibly be corrected by using a material that would not bend under the fluid pressure such as steel and including a chamfer on the edges of the plate and raised friction pad similarly to the 2H plate to further avoid performance degradation due to

debris under and around the plate. These issues severely compromised the pressure measurements over the course of testing. However, the available testing data suggests that this plate had a fairly low pulsation energy. This was likely due to the very small change in flow area between a fully open and fully closed configuration of the plate (approximately half of one hole area difference in area). When the plate would stick it would also tend to stick in the orientation with two holes open since this was a lower pressure configuration than when only the one offset hole was open.

The 2HL plate was by far the best performer in terms of pulsation energy. A simple visual inspection of the tests showed that only this plate produced a pulsating force significant enough to rock the platform that secured the bit. Despite being constructed of the same 6061 aluminum as the 3H plate the pulsation performance was fairly consistent. However, by the end of the 100 seconds of testing it was apparent that the plate would occasionally stick for a few tenths of a second before continuing to spin normally. The same circular gouges as seen on the 3H plate were observed along the bottom and sides of the 2HL plate indicating that the pressure was warping the plate leading to an increased frictional surface area and premature wear. An important design feature that may have enabled this plate to continuing spinning despite this lack of material stiffness was that the holes were staged so that as one hole was beginning to close the next hole would begin to open. The effect of this was to overcome to resistance to hole closure that could create erratic pulsation and increased spinning resistance. Due to the massive flowrate and fluid pressure within the bit the force required to close off each flow path as the plate spun was difficult to overcome for plates other that the 2HL plate. The 2HL plate also had long enough hole openings that a large amount of fluid passed through the outside bit nozzles instead of only the center nozzles as was the case for the 2H plate. Despite the plate warping and the resulting high friction this plate clearly demonstrated that elongated holes with properly staged hole opening and closure could produce a fairly consistent pulsation profile with a high energy.

After observing the performance of the 2HL plate the 1H plate was built in an attempt to capitalize on the results of the first 3 plate tests. With this in mind the plate was created out of brass to reduce galling due to debris and made with only one long hole so that even at high plate RPMs the fluid channels would be open long enough to allow fluid flow. The outside diameter of the plate was also reduced by 0.127 mm (5/1000 in) and the friction pad raised by 2.5 mm (1/10 in) to prevent debris induced plate sticking. Visual analysis during testing indicated that the plate was spinning quickly and consistently and there was a clear opening and closing of each outer nozzle flow. Fig 34 shows this change of fluid path; as the plate rotated each of the five outer nozzles opened and then closed. In this image nozzle one closes and then nozzle 4 opens indicated by the red trace of the fluid jet.

Figure 34: 1H plate changing fluid path

4.4 Open vs. Closed Flow Area

Despite this changing flow path seen during testing of the 1H plate upon analysis of the pressure data the pulsation energy appeared to be very low, an observation echoed by the plot of filtered pressure vs time of each plate. This was due to negligible change in open vs. closed flow area of

this plate design. While the other plates had flow area changes ranging from one to two hole areas the 1H plate continuously had 3 holes open for fluid flow. Despite the actual nozzles involved in flow changing as the plate rotated, one hole opening was always matched by another closing and because the fluid pressure is primarily a function of open/closed area the pressure fluctuation was very low. While this plate could create very efficient cleaning of cuttings during drilling due to the consistent rotation of a high pressure zone and low pressure zone under the bit as the plate spun the effect of pressure pulsation would be minimal indicating this design might not be the most efficient. However, by decreasing the plate diameter and friction pad height a reduction in sensitivity to fluid debris was achieved and the elongated holes enabled fluid flow through the outer nozzles even at high rotational speed. As a comparison the difference between the fully open and fully closed areas for each plate was calculated and a visual example of this difference is shown in Fig 35-37.

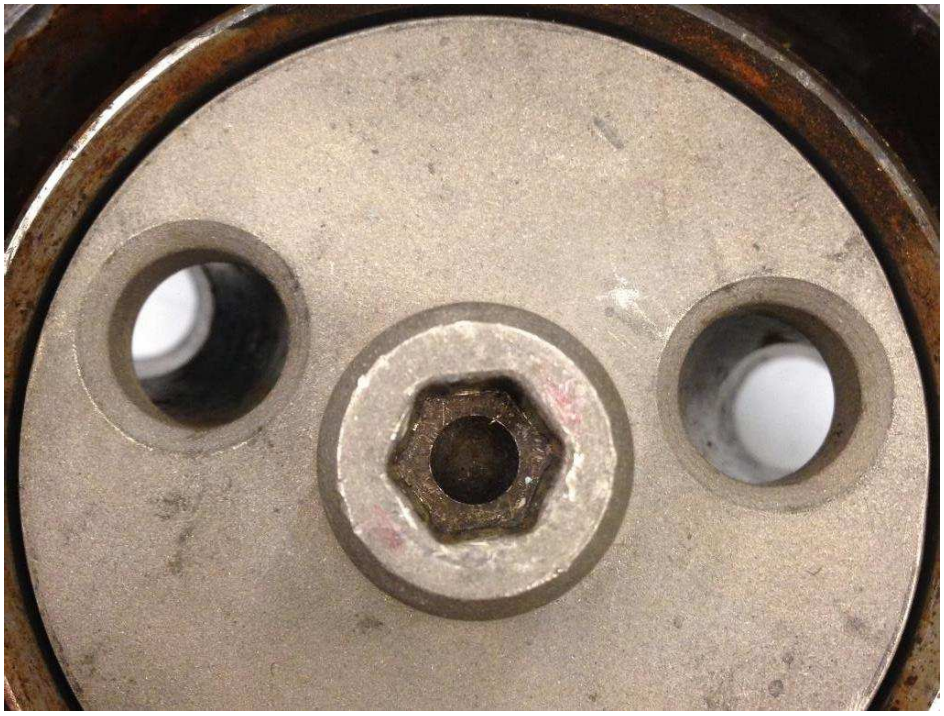

Figure 35: "Fully open" 2H plate

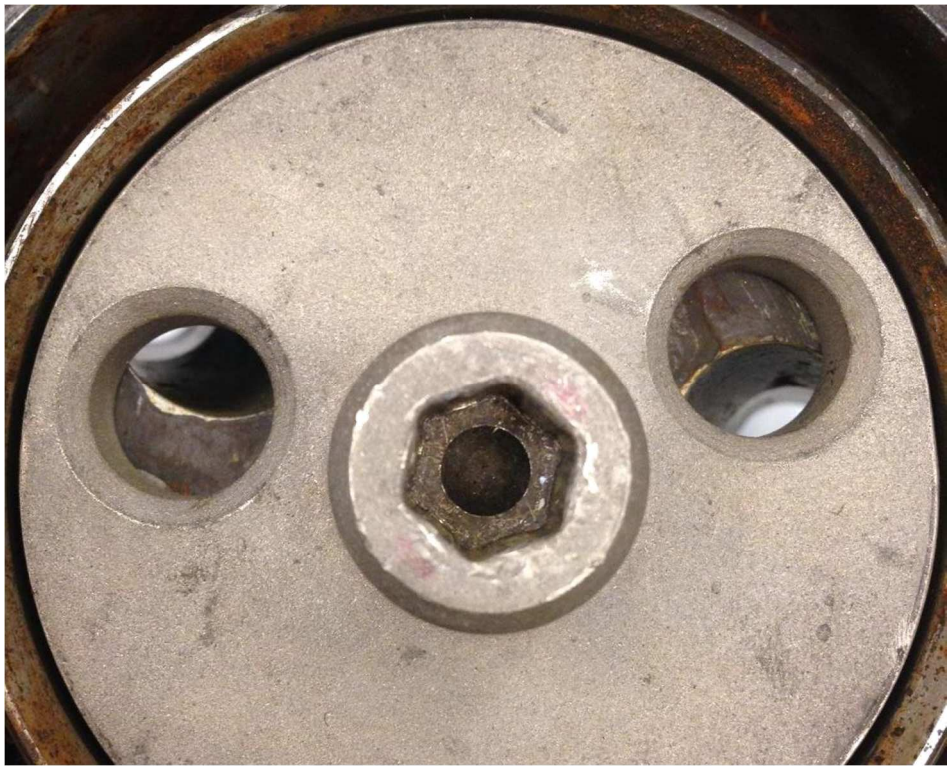

Figure 36: "Half open" 2H plate

Figure 37:"Fully closed" 2H plate

The area difference for each plate in terms of one hole area is shown in Table 6.

Plate	Area Min, in²	Area Max, in²	Difference, in²	# Holes
2H	0.00	0.42	0.42	2
2HL	0.16	0.40	0.24	1.15
3H	0.31	0.42	0.10	0.5
1H	0.63	0.63	0.00	0

Table 6: Plate max/min area difference

4.5 Pulsation Power

During this analysis it was clear that with the pressure component due to the pump was dominant for most of the test data and once removed the pressure fluctuation amplitude was greatly reduced for all plates other than the two-hole long design (2HL). To quantify the differences in pressure pulsation amplitude between plates it was necessary to create one metric that combined and described the pressure characteristics of most interest. The pressure pulsation amplitude was not an unbiased comparison value due to the difference in pressure profile characteristics and flowrates; for example, a narrow peak would not contain the energy of a broad peak despite having the same amplitude and the greater the flowrate obtained the greater the pulsation power which would be achieved. The term "Pulsation Power" hereby referred to as "Power" was calculated as the standard deviation of the filtered pressure data multiplied by the flowrate as given in Eq. (2).

$$Power = Std.\big(P(t)\big) * Q \tag{2}$$

While it would be possible to create a more sophisticated term which could weight each individual data point more or less depending on the variance from the mean, the nature of this testing only required a rough comparison tool which could quickly reduce large data sets into one comparable value.

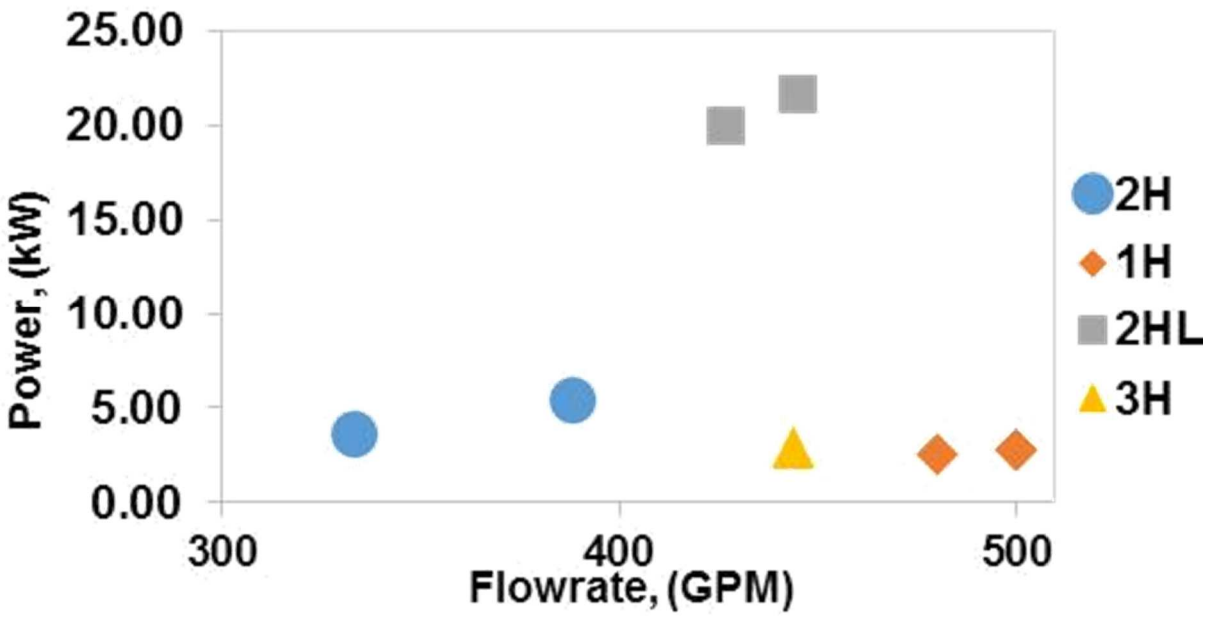

Figure 38: Pulsation power comparison by plate plot

Figure 38 compares the calculated values obtained during testing for the power of each plate. Only the tests conducted at maximum pump output are included as these tests most closely simulate field conditions and at pump outputs much lower the plate would not spin. The 2HL plate clearly outperformed the others in terms of power and there was a slight positive relationship between flowrate and power output for each plate individually, which would be expected. The variance between data points with the same plate are due to operating the pump at a slightly higher output for the second tests performed with each plate.

CHAPTER V

MODELLING

5.1 Sinusoidal Wave Modelling

The first step toward predicting future plate performance was to understand the effect of both operational changes such as flow rate and interrupter plate design changes on the following pressure metrics:

1. Pulsation amplitude, (A)
2. Pulsation frequency, (B)
3. Average pressure, (C)
4. Pulse waveform characteristics (Shape, ratio of open to closed holes per revolution)

To this end a model was created that attempted to simulate the pressure response due to the flow area change as a sinusoidal wave. By comparing the predicted pressure metrics to those obtained during testing this analytical model was refined and used as a prediction tool to compare the effects of different operating parameters on the pressure metrics of interest, as well as validate the pulsation performance. The pressure fluctuations created by the DBB can be approximated as a sinusoid wave with amplitude (A), frequency (B) and average pressure (C) as shown in Eq. 3 and Fig. 39.

$$P(t) = A * Sin(Bt) + C \tag{3}$$

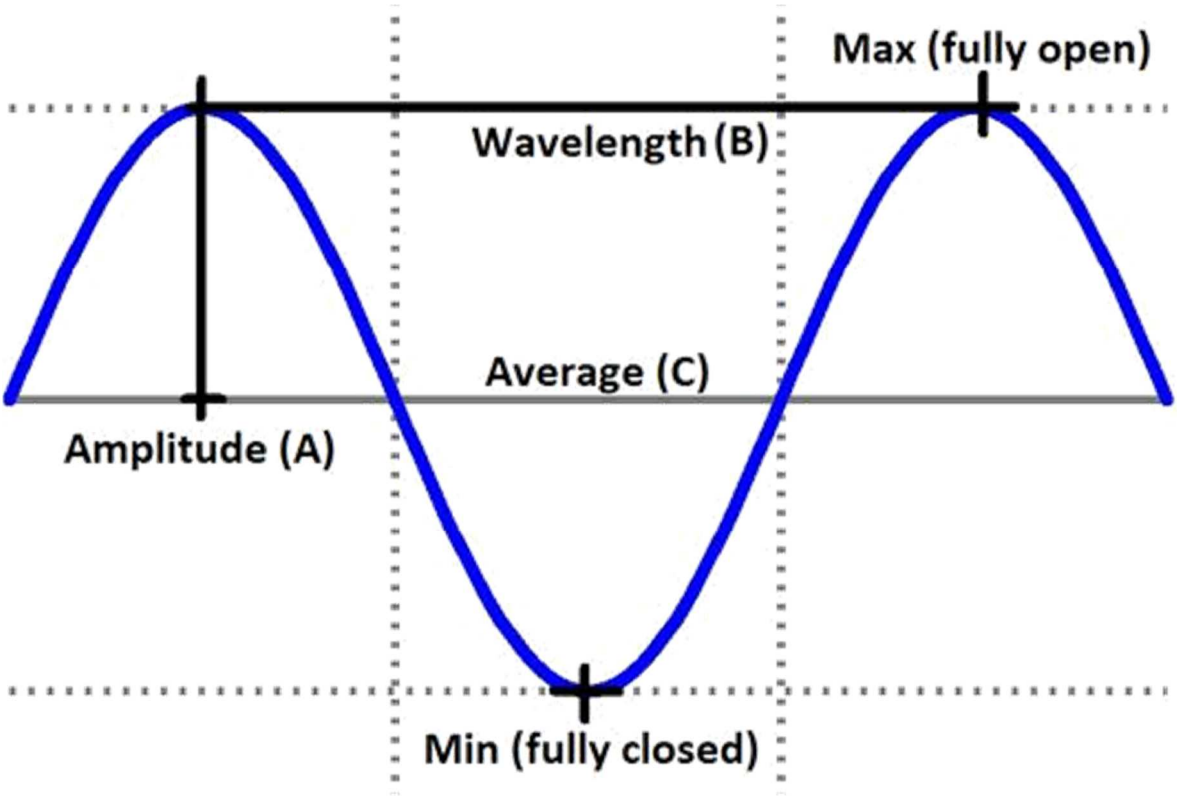

Figure 39: Sinusoid pressure modelling variables

While this is a simplification of the actual waveform created, it is convenient in that it allows for a simple comparison of the three metrics important for design optimization. Pressure through a restricted opening in field units is given by Eq. 4 from Leonov & Isaev (2010).

$$\Delta P = \frac{Q^2 \rho}{12031 C_D^2 A_n^2} \tag{4}$$

Here Δ is the pressure drop across the opening, Q is the flowrate, is the fluid density, is the discharge coefficient, "12031" is a conversion factor and is the flow area. Using this equation, the values for A and C were calculated using the maximum, minimum and average flow area for one revolution of the interrupter plate. The amplitude, "A" was defined as the difference between the maximum and minimum pressure divided by a factor of two and the average pressure was approximated as the sum of the maximum and minimum pressure divided by a factor of two. This was only an initial approximation as calculating the actual average pressure would require a

calculation of the area continuously as the plate rotated and would require simulation. The frequency component “B” had to be extracted from the experimental data. It was difficult to predict the effect of design changes on the rotational frequency of the plate as internal friction plays a large role in the rotational speed of the interrupter plate. Instead, the term “B” was extracted from the spectral analysis of the testing by taking the frequency value of the dominant peak and multiplying by a factor of 2π to obtain the frequency in radians. Initially, an attempt was made to use the manufacturer rotor stator mud motor performance curve to predict the frequency of pulsation, however, in the previous testing conducted in 2013 the motor was cut in half in an attempt to reduce the pulsation frequency. The effect this modification would have on the stall torque and performance curve was unknown, however, if the reduction in motor length by a factor of ½ led to roughly the same factor of ½ being applied to the motor metrics and performance curves then the torque required to spin the plate during recent tests must have been very high as the RPMs achieved during testing of the motor were on the order of 40-80 RPM and a value of this low indicates the motor was performing at near the maximum torque and minimum RPM capable.

1-11/16" 5/6 4.4 STAGE

169R5644

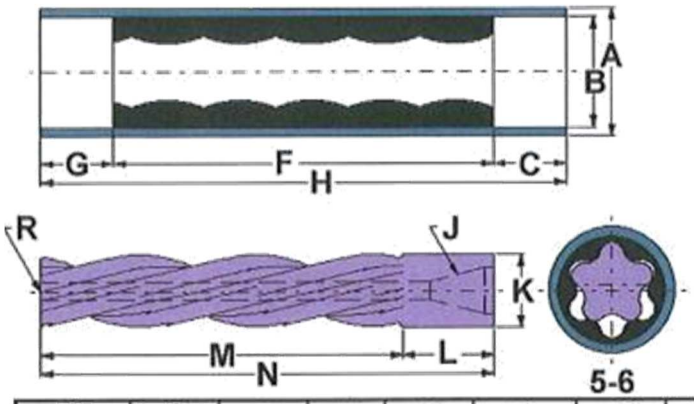

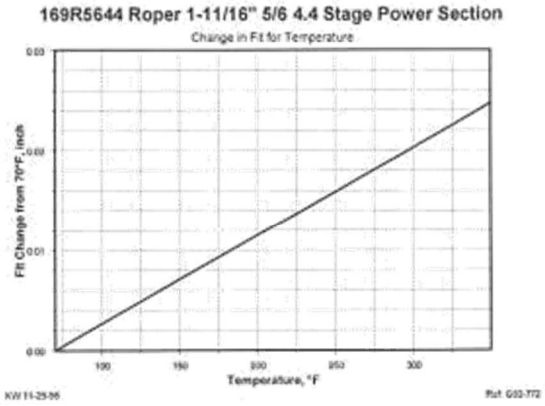

A	B	C	F	G	H	M	N	L	K	R	J
1-11/16	1-3/8	4-1/4	74	4-1/4	82-1/2	75	79	4	1	—	—

	STD	OVS	2XOVS
STATOR MAJOR DIAMETER	1.192	1.202	1.229
STATOR MINOR DIAMETER	0.844	0.854	0.881
ROTOR MAJOR DIAMETER	1.018		

APPROX STALL TORQUE	225 FT-LBF
ROTOR ECCENTRICITY	.087
ROTOR WEIGHT	20 LBS.
STATOR WEIGHT	21 LBS.

PERFORMANCE DATA

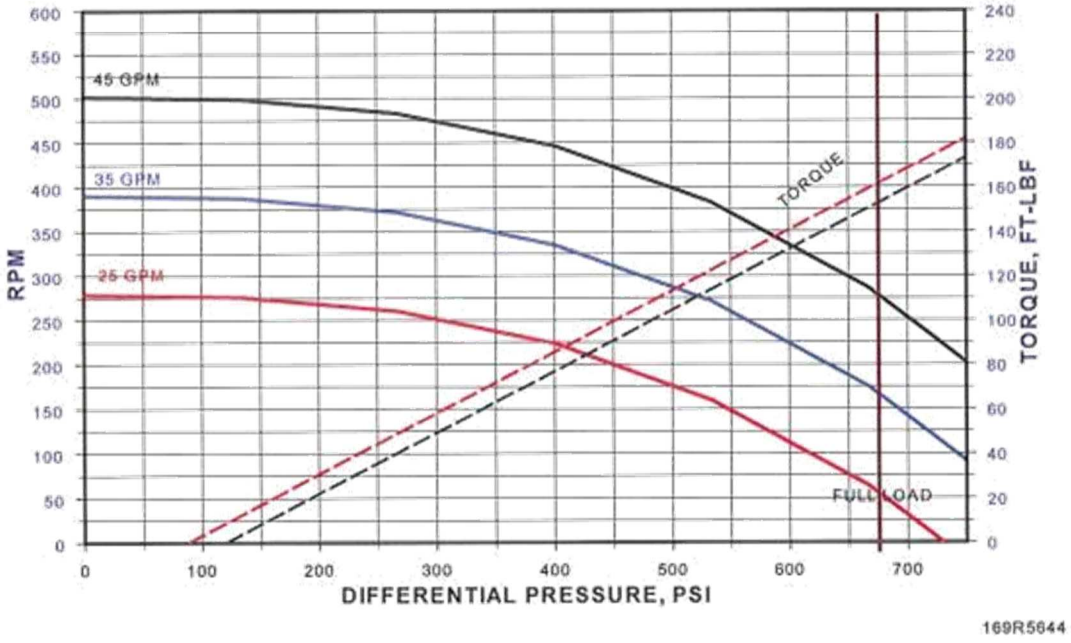

Figure 40: Mud motor performance curve and specifications

A summary of the calculated values of “A”, “B” and “C” is given in Table 7 for the 2HL plate.

Amplitude, “A” (PSI)	Frequency, “B” (Radians/sec)	Ave. Pressure, “C” (PSI)
217	8.6	991.5

Table 7: Model "A", "B", and "C" values for 2HL plate

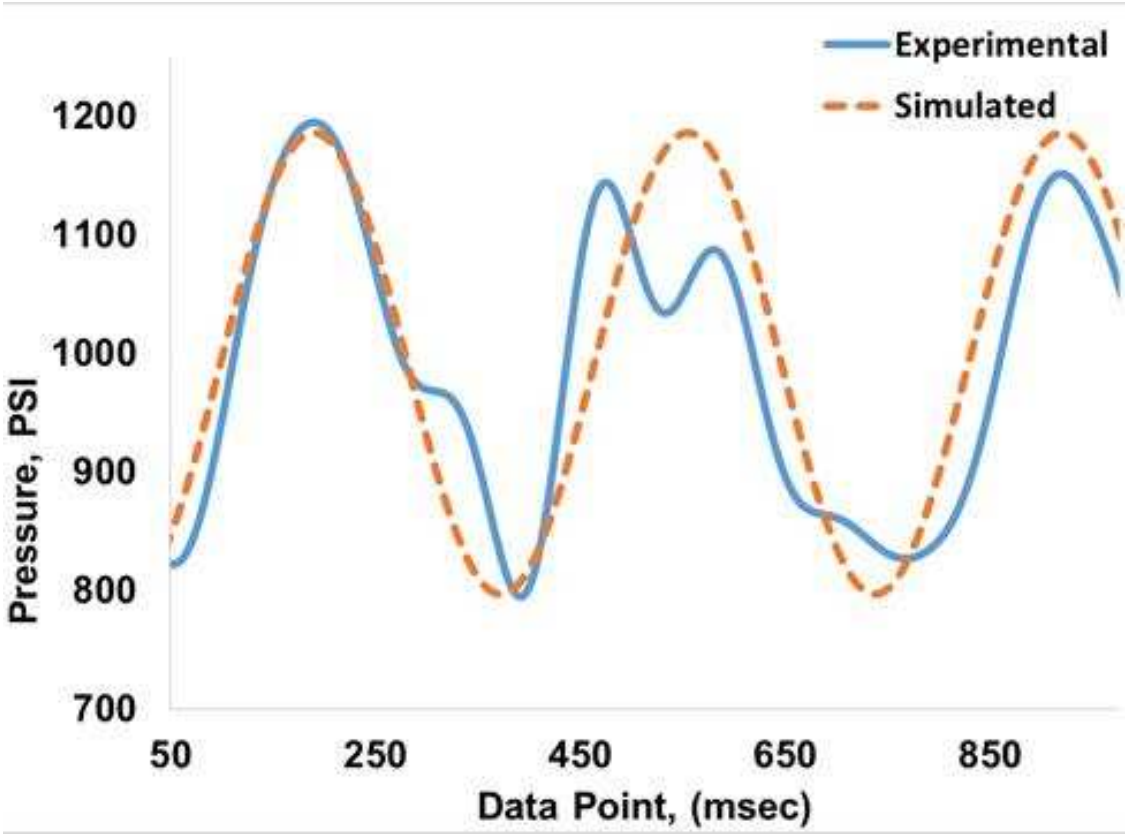

Figure 41: Experimental vs. simulated pressure data for 2HL plate using sine wave model

A comparison of the simulated pressure and the experimental pressure for a test is shown in Figure 41. The model metrics were adjusted to match to the experimental data metrics by modifying the discharge coefficient until the difference between the model pressure metrics (average pressure and pulsation amplitude) and experimental data was minimized. An analytical solution would be both difficult to obtain and possibly more error prone than this method as the term accounts for every flow direction change, surface roughness and area change between the location of the pressure measurement and return to ambient pressure upon exiting the nozzles.

While the model fails to follow every deviation in the experimental data the important metrics, A, B and C are matched very closely leading to a simple set of values that can describe the pulsation performance as well as simulate the actual pressure response. During future testing this method of analysis could allow for a simple comparison of different plate designs tested experimentally as well as possibly predict the performance of untested interrupter plate designs. However, in order to more fully understand and predict the performance of a plate design a more sophisticated model was needed which could accurately predict pressure profiles beyond simple sine waves, such as the double peak wave seen during testing of the 2HL plate.

5.2 Interrupter Plate Modelling

In order to overcome the limitations of the sine wave approximation a new model was created which could more closely match the results from experimental testing to reduce the need for further testing and allow for optimization of the plate design based on a calculation of fluid pressure. This model operated by calculating the instantaneous flow area as a function of plate geometry, time and rotational frequency. By using a small time step between calculations a near continuous approximation of the flow area was obtained. By approximating the rotation of the plate holes over the stationary holes in the DBB as a linear translation an equation for the instantaneous overlapping area of two circles was obtained in Eq. 5 with variables shown schematically in Fig. 42.

$$A = 2\left(\frac{2\pi r^2}{360} cos^{-1}\left(\frac{d}{2r}\right) - \frac{d}{2}\sqrt{r^2 - \frac{d^2}{4}}\right) \quad (5)$$

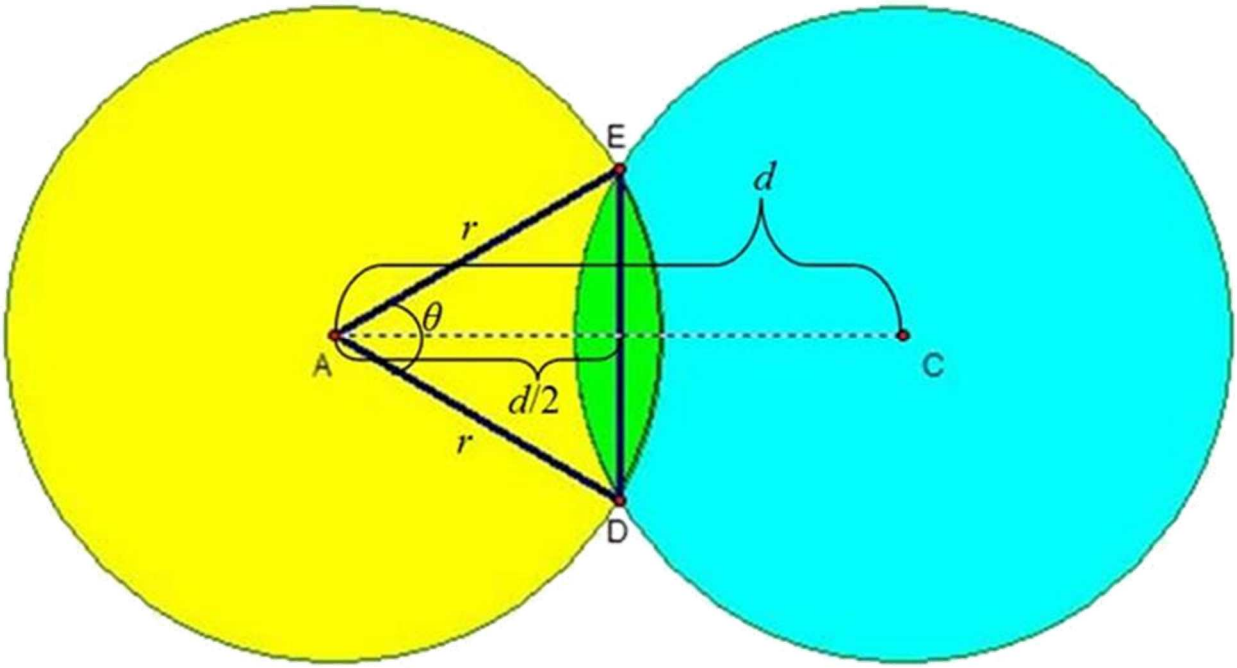

Figure 42: Area calculation diagram

The overlapping area shown in green was calculated as two times the area of the sector (A_{sect}) minus the area of the triangle AED (A_{tri}). By stepping through "d" at very small increments a curve of area vs. time could be obtained. The area of the sector and triangle are shown in Eq. 6 (Weisstein, 2010) and Eq. 7.

$$A_{sect} = \frac{2\pi r^2}{360}\cos^{-1}\frac{d}{2r} \tag{6}$$

$$A_{tri} = \frac{d}{2}\sqrt{r^2 - \frac{d^2}{4}} \tag{7}$$

The overlapping area is then simply twice the difference of these equations. Using the pressure drop through a restricted opening equation from earlier (Leonov & Isaev, 2011) a calculation of the pressure as a function of this area was obtained for one hole. The next task was to accurately reproduce the staging of each hole opening and closure for any plate design based on a simple set of user inputs including:

- Time step (sec), delta_t
- Hole radius (in), r
- Radius of hole center to plate center (in), R
- Number of holes, holes
- Length of hole opening (in), L
- Distance between hole centers (in), D

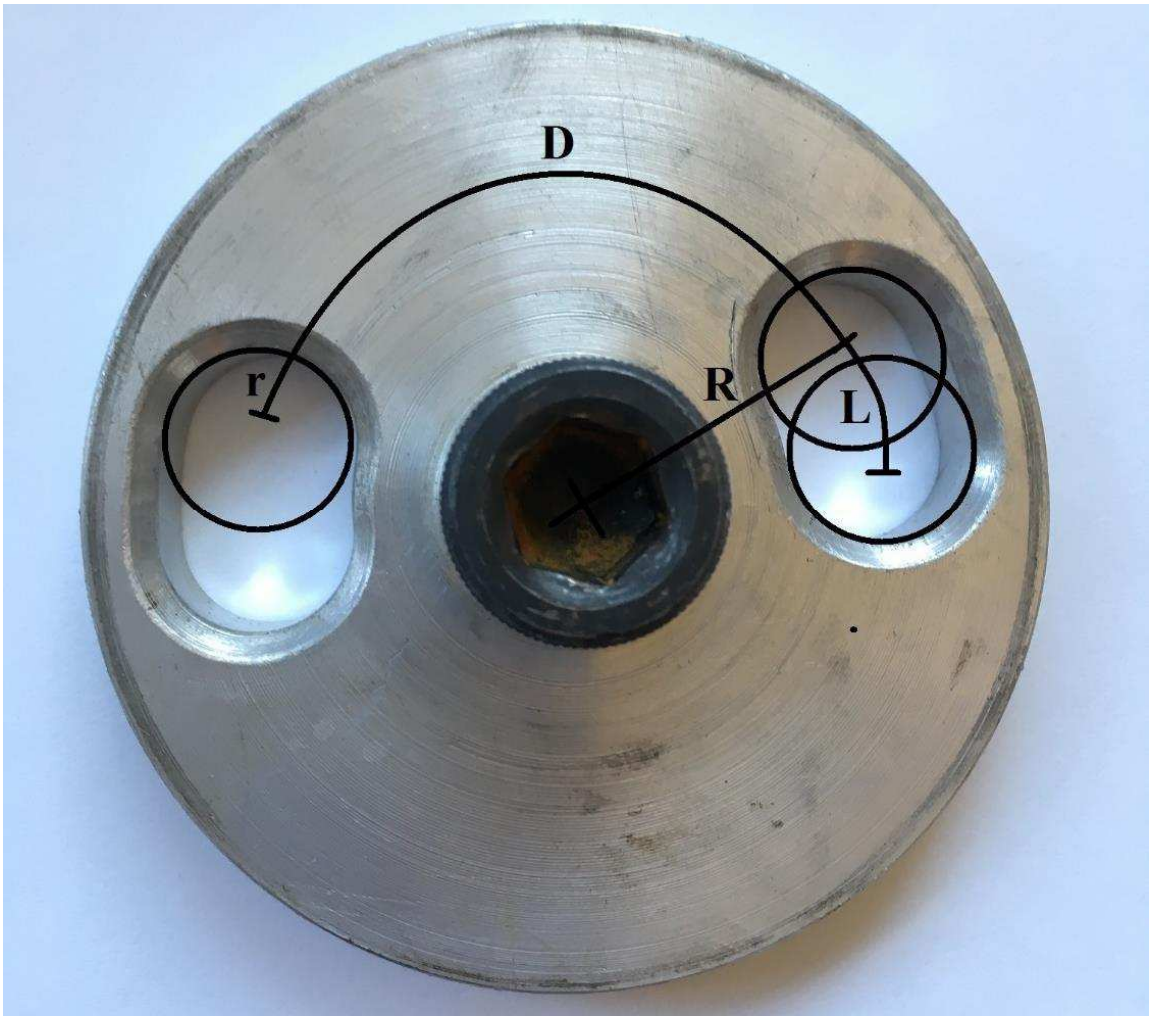

Figure 43: User input plate geometry diagram

The inputs listed above correspond to the dimensions shown in Fig. 43. The user would also input the following:

- Shaft frequency (Hz), freq
- Flowrate (GPM), Q
- Mud density (PPG), density
- Central (always open) nozzle radius (in), r_o

Using these inputs the code would follow these steps:

1. Calculate the velocity of each hole center, v
2. Calculate the linear distance between each hole edge, s
3. Calculate the null flow area (the area of the always open nozzles), A_o
4. Calculate the time required for 1/5 revolution of the plate (since there are 5 nozzles which can open and close), t_1
5. Calculate the starting area for one hole starting at the minimum open hole area, A_o
6. Create the vector of distances (d in Fig. 42) between the plate hole and bit hole as a function of time step and plate geometry for the opening and closing of the hole, d(i)
7. Calculate the area as a function of the distance vector, A(i)
8. Simulate one revolution of the plate by overlaying each hole area as a function of time and properly staging the opening and closing of each hole relative to the first hole
9. Add in the null flow area from the always open nozzles
10. Calculate the pressure as a function of the area vector, P(i)
11. Plot the pressure for one plate revolution

The model was adjusted to match to the experimental data by modifying the discharge coefficient until the difference between the model pressure metrics (average pressure and pulsation amplitude) and experimental data was minimized. As previously discussed an analytical solution for the discharge coefficient would be both difficult to obtain and possibly more error prone than this method as the term accounts for every flow direction change, surface roughness and area

change between the location of the pressure measurement and return to ambient pressure upon exiting the nozzles. An example of the plot produced for the 2HL plate is shown in Fig. 44

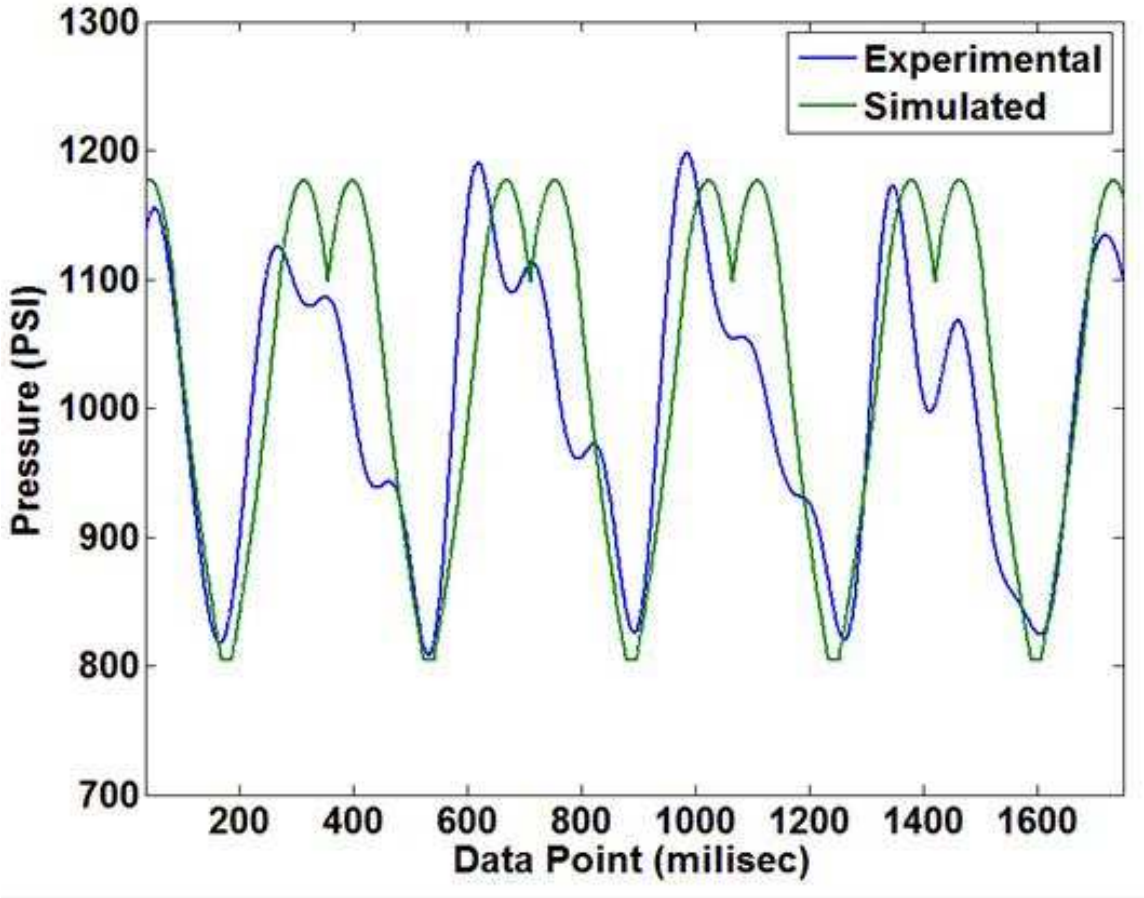

Figure 44: Experimental vs. simulated pressure for 2HL plate using area model

While there is clearly some deviance between the simulated and experimental results many of the important pressure metrics are captured as well as the wave shape. The average pressure and amplitude of pulsation matches closely and the multiple peak wave shape is even predicted. However, the model predicted two peaks of equal magnitude while the experimental data had some peaks with only one peak while others had two or three peaks with each pulse of descending magnitude. Currently these differences cannot be fully accounted for, however, they are likely due to some sort of coupling effect between the pump and bit. It is possible that each initial pulse resonated between the pump and bit causing the decreasing magnitude pulses seen in

some of the data. It is also possible that these multiple peaks are an artifact of the plunging action of the triplex pump used during testing that was not fully filtered out. There was also frequently a low pressure zone following each fifth pulse that lasted for approximately the same length of time as one pulse in the experimental data. This 5 pulse pattern likely reflects some type of inconsistency in either the plate geometry, or friction that occurred once per revolution of the interrupter plate as one revolution produced five pulses.

The 2H plate modelling did not match the experimental results as closely as the 2HL plate. Furthermore, the discharge coefficient used in the model that most closely matched the experimental results was very low (0.44) compared to the coefficient used for the 2HL plate (0.89). This was attributed to the lack of fluid flow through the outside nozzles due to the high rotational speed of the plate and a lack of an elongation of the plate holes. As previously discussed this invalidated the design, which led to a poor modelling match.

The 3H plate had a tendency to become stuck with the 2 holes open during testing. This was attributed to both the debris induced friction increase as well as the lower average pressure when the two matched holes were open instead of only the one staggered hole. This led to the data being of insufficient quality to draw useful conclusions from regarding the pressure metrics. However, by staggering the holes so that the closing of the matched holes was slightly preceded by the opening of the staggered hole and by lowering the plate spinning friction this design could be viable. The analytical model predicted a frequency of twice the other models due to the staggering of the holes with a distinctive two amplitude set of peaks.

The 1H plate was predicted to have no change in pressure because while the nozzles which were open changed the total number of nozzles open did not. This was predicted by the model. However, this plate was machined on site during testing and as a result was not modelled beforehand. This lack of pressure change was verified by experimental data and although there

was a very slight (10-30 psi) pressure fluctuation this was likely due to the effect of the fluid path through the nozzles changing and not due to the area as the area remained constant.

By comparing the model predictions to experimental data it was clear that this model could only be used as a prediction tool for plate designs that performed as expected and did not suffer from one of the difficulties (spinning too fast, becoming stuck) that the 2H and 3H plates exhibited. With this said, the model was able to capture the wave shape much more closely than the sine wave model and could be a useful tool in the analysis of future plate designs.

5.3 Power Optimization

Experimental testing allowed for an evaluation of plate materials, friction pad materials, and edge geometries. However, the testing was limited in what could be evaluated in terms of power production. It was clear that the 2HL plate produced the greatest power so design optimization of this plate design was conducted. To this end the pressure-area modelling code was used in a power sensitivity analysis to predict the effect of plate geometry and operating conditions on the power produced. By changing each variable independently to 1/3, 2/3, 4/3, and 5/3 of the value of the experimental test the major contributors to power were evaluated as shown in Fig. 45.

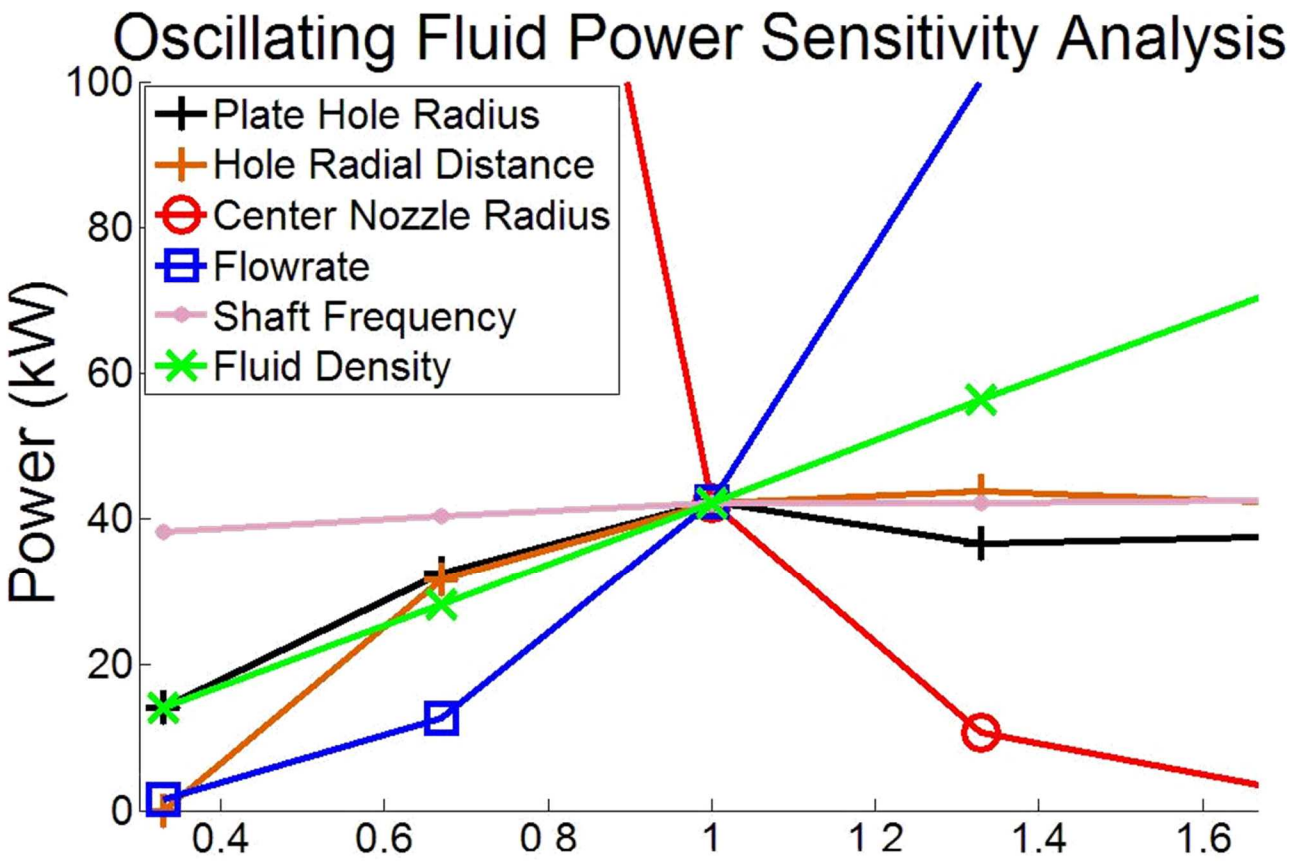

Figure 45: Power sensitivity analysis for 2HL plate design using area code

The greatest effects were due to the flowrate, fluid density and center (always open) nozzle radius. However, during drilling the flowrate and drilling fluid density are often constrained by operating conditions and cannot be changed significantly (Liz-Losada & Alejano, 2000) so the only design variable with a strong positive modifiable effect on power was the center nozzle area. By reducing the radius of the two center nozzles, which are always open to flow, the difference in flow area as a fraction of the average flow area between a fully open configuration and fully closed configuration became larger leading to increased peak pressure. In fact, the peak pressure approached infinity as the minimum flow area approached zero; however, this is not practically applicable since the pump output limits the maximum obtainable bit pressure. What this did mean, is that if a plate design such as the 2HL plate were used without any center nozzles the power could be increased substantially beyond what was measured in experimental testing.

Furthermore, because there would always be an area open for flow due to the elongation of the holes with this plate design, possible negative effects such as water hammers could be avoided. However, it is important to consider the effect this modification could have on bit cleaning. As the center nozzle diameter is reduced the pressure at any flowrate is increased and in typical drilling operations effective bit cleaning is related strongly to flowrate. So there must be a balance between a large enough average area to allow an adequate flowrate and a small enough minimum area to increase the pulsation amplitude and thus the power. Despite the usefulness of this sensitivity analysis for design optimization it failed to combine all aspects of the pressure pulsation. For example, Fig. 46 shows the effect of changing the size of interrupter plate holes (and corresponding nozzles in the bit). While this has minimal effect on the power of pulsation the effect on bit cleaning could be dramatic because the average pressure, flowrate, amplitude and length of each low pressure zone following a pulse is modified. This also demonstrated the highly modifiable nature of this design; by only changing one geometry a wide range of performance characteristics could be achieved. It is important to note that the channel connecting the holes in the interrupter plate to the nozzles on the outside of the DBB would have to be at least as wide as the plate hole diameter to achieve these design modification effects otherwise the channels are a choke point instead of the plate holes.

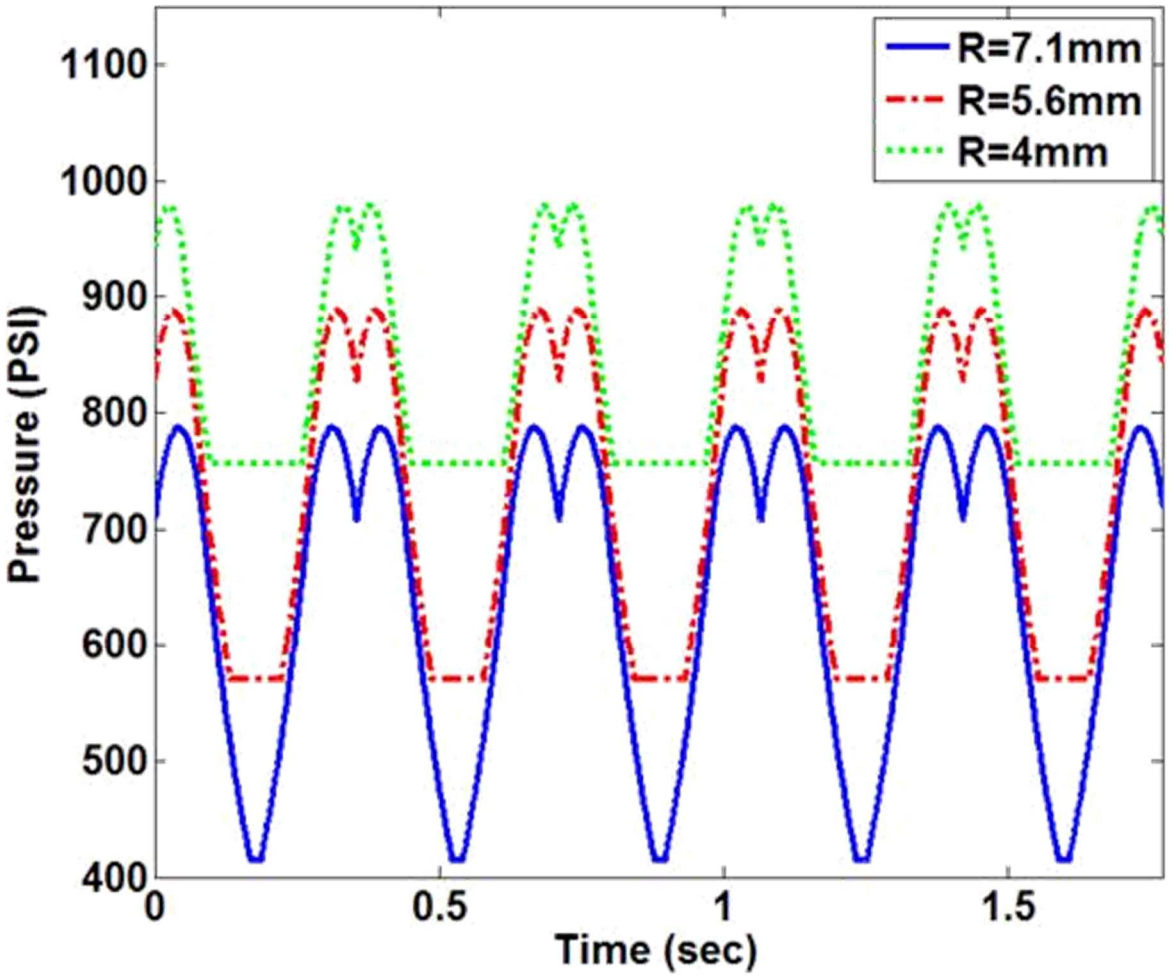

Figure 46: Plate hole radius effect on pressure curve

5.4 Design Recommendations

Using the results and observations from experimental testing as well as analytical modelling a list of design factors leading to both positive and negative outcomes was created to aid in future design recommendations.

Positive Design Traits:

- Elongated interrupter plate holes
- Steel plate material

- Carbide center disk
- Slightly raised center disk
- Chamfered outer plate edges and holes
- Minimal central (always open) nozzle area
- High flowrate and fluid density

Negative Design Traits:

- Staggered interrupter plate holes
- Steel center disk
- Mud motor with high required pressure

This list was created primarily from observing what didn't perform well during experimental testing. There are also several design modifications that while not tested or modelled could also minimize some of the issues observed during testing. One of the primary problems during testing was due to debris building up around and under the interrupter plate. When tested the DBB did have a conical filter encompassing the flow interrupter plate however the slits through which fluid flowed through were 2.5mm wide which allowed many fairly large pieces of debris to pass as shown in Fig 47.

Figure 47: Conical filter in DBB

It would be possible to attach a finer mesh to this filter cone to keep debris from causing the interrupter plate sticking or wearing out prematurely. By reducing the size of debris which could come into contact with the interrupter plate the consistency and longevity of the pulsation production could be enhanced significantly. And because the flow through the central (always open) nozzles bypass this filter any debris that could not pass through the mesh would be pushed down the sides of the conical filter and expelled through the central nozzles, reducing any

tendency of filter clogging. Another primary concern for this design which was observed during testing was the difficulty in closing open fluid paths and in getting fluid through the plate holes; an issue that occurred increasingly as the plate rotational speed increased. This problem caused the 3H plate to get stuck in the open configuration occasionally when debris increased the spinning friction and also likely caused the delay in hole closure observed after several of the pulses for the 2HL plate. By including a wedge or scoop shape on one side of each plate hole as shown in Fig. 48 such that the flow of the fluid over the plate and through each hole exerted a torque on the plate more consistent closing of holes already open could be achieved.

Figure 48: Wedge on interrupter plate

In order to even further increase the plate rotational speed bearings could be installed under the rotation pad so that instead of a carbide on carbide friction the bearings would rotate. If this were implemented it would better to use a material with a high frictional coefficient so that rotation between the surface of the plate and the rotational pad occurred simultaneously leaving only the bearings to roll. While the analytical model was useful to aid design decisions ultimately it was impossible to verify the performance of any new design without experimental testing. By studying the design of successful tools already tested and in use such as those discussed in the

literature review section of this paper, the efficacy of several design modifications not tested in this design could be substantiated.

The pressure chamber shown in yellow in Fig. 49 below could be altered so that its geometry amplifies the pulsation similarly to Fu et Al. (2012) and Cui et al. (2013) both of which employed the use of a resonant chamber.

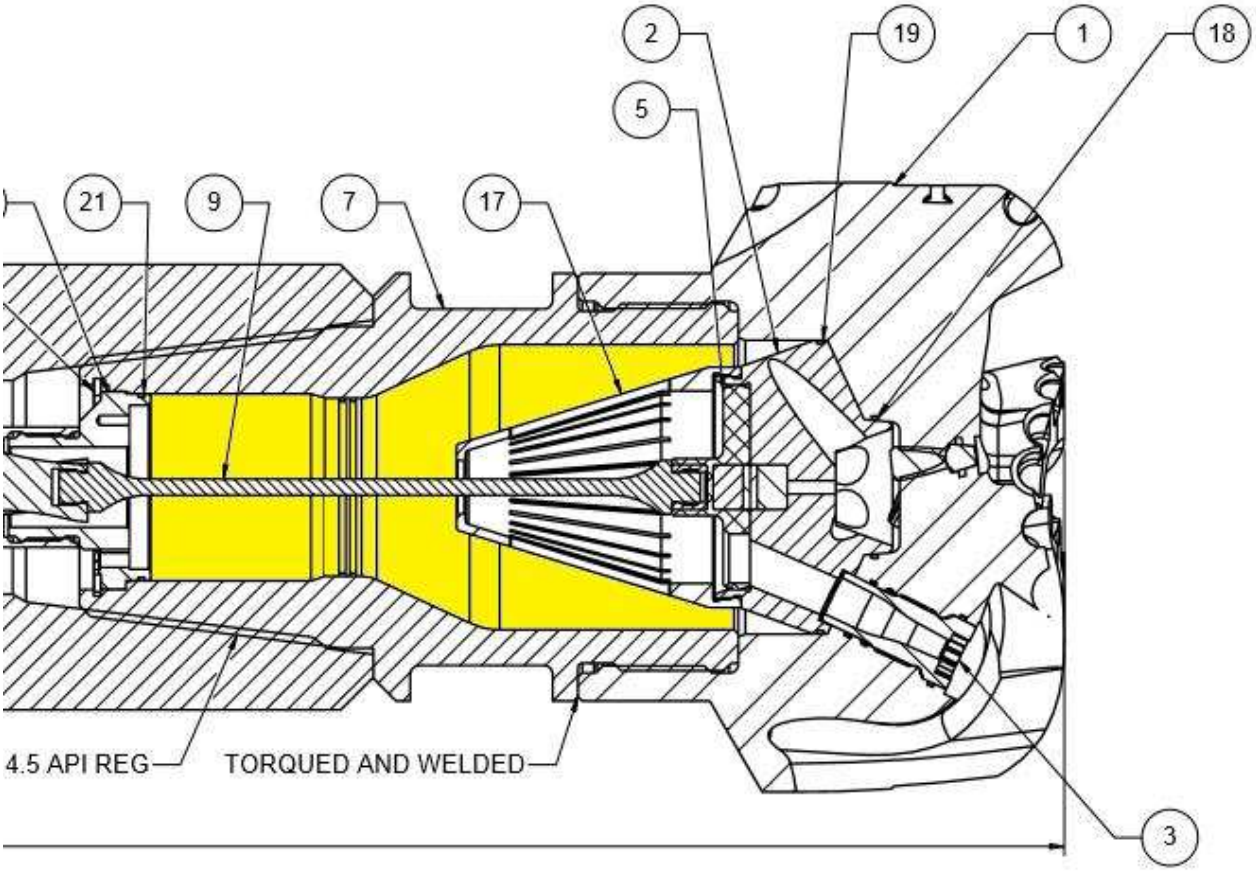

Figure 49: DBB pressure amplification chamber

In order to improve the reliability and lifetime of this design the interrupter plate design mechanism could be reversed so that instead of the plate with holes spinning on top of a fixed set of nozzle holes an interruption mechanism with a fixed geometry could spin over a changeable plate with hole geometry the same as the interrupter plate designs in the DBB as shown in Fig. 50. This could allow for the creation of a stronger more durable interruption mechanism to be

used which would be compatible with all interrupter plate designs and possibly less prone to binding due to debris. And by keeping the plate stationary more plate designs could be used since the stresses on the plate would be reduced. This design would still allow for a highly customizable pulsation generation without any major design changes while increasing the robustness of the design.

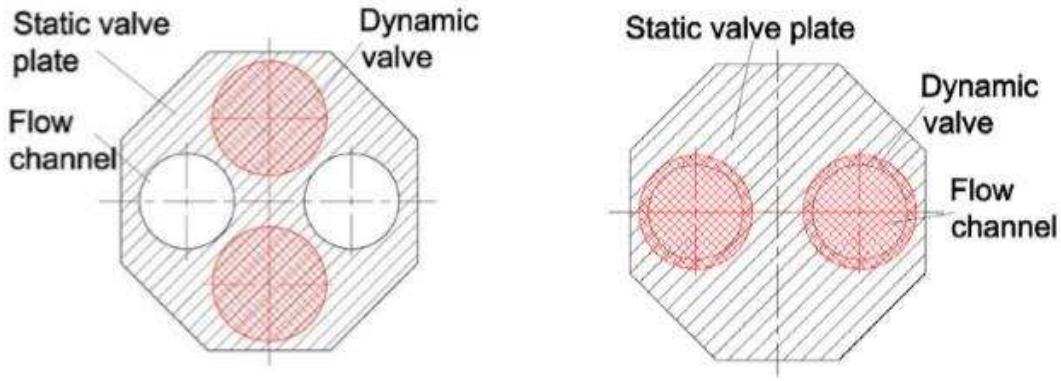

Figure 50: Pulsation mechanism design change (Cui et Al., 2013)

Lastly, if the performance benefit demonstrated by the cavitating nozzles described in Gensheng et al. (2011) could be integrated into the DBB design it is possible the pulsation effect could be further increased leading to an even greater ROP than has been obtained by previous designs. They could be installed along the flow path from interrupter plate to nozzle outlet in the current DBB design however testing is needed to verify that the intermittent flow through each nozzle that occurs during use of the DBB could generate and sustain these self-cavitating pulses.

CHAPTER VI

CONCLUSIONS

6.1 Summary

Any improvement over traditional technology in the field of drilling for natural resources is important because of the high operational cost associated. This is historically an active area of research, but the study of new bit technologies and designs is fairly limited due to the inherent difficulty in determining the effect of a large number interrelated variables on performance. A methodology for experimentally testing further DBB designs was established and used to test the performance of the DBB. By recording repeatable data sets for a number of different internal plate designs and operating conditions the method was validated and an analysis of the performance of the DBB enabled. Several methods of analysis were used to quantify various performance related characteristics of the DBB; these methods could be used for future research as a benchmarking system to compare future DBB designs. This allowed for the development of the term “power” as a reliable metric of the pulsation strength, which was used to optimize bit design. Combining these steps could allow for a less biased and more useful comparison of pulsating bit designs. This process was used to test a new DBB design whose efficacy is based on previous research which indicated that several of the operational characteristics of this design lead independently to an increased ROP. Furthermore designs with a different pulsation

mechanism but similar pulsation metrics to the DBB have been tested in the field and led to substantial improvements in bit life and ROP

6.2 Future Recommendations

This research is the first step towards the ultimate goal of having a highly controllable drilling system in which the pulsation characteristics are optimized with regard to maximizing the overall drilling ROP. In order for this goal to be realized further study must be completed in several areas:

- The DBB design must be modified to increase the robustness of the design. This could be accomplished through any one of several means. For example, a modification of the interrupter plate to reduce binding and wear as detailed previously could increase reliability. Further testing would have to be done after any design modification to ensure that the modelling tools used could still replicate experimental results.
- The response of the mud motor to variations in inlet flow areas must be studied as well as the possibility of changing the current mud motor for one with a larger operating range. This would enable data collection across a larger set of operating conditions. Ideally, a motor with a low start up pressure, high output torque, and high, controllable flowrate would be implemented.
- The response of the interrupter plate pulsations to varying mud motor outputs and pump outputs should also be studied. Since various types of pumps are used in the field the coupling effect between the pump pulses and the bit pulses should be analyzed to ensure that the expected DBB performance could be obtained regardless of the type of pump used for a drilling operation.

- The DBB should also be tested extensively in actual drilling operations while the pressure at the bit is measured in order to ascertain the differences in pulsation in above ground and downhole testing.
- Lastly, a detailed analysis of rock response to low pressure pulsation is needed in order to allow the DBB pulsation to be optimized with regard to each rock lithology.

6.3 Conclusions

- Vibration has been proven to increase bit life and ROP while enabling better control of the bit face and more accurate WOB measurements.
- Vibration due to cavitation and flow interruption has been proven to lead to increased ROP and bit life in numerous field tests.
- The control of pulsation frequency has been demonstrated to be a key factor in increasing ROP during drilling.
- The experimental set-up used to test the DBB allowed for high resolution recording of pressure data which was used to analyze the bit performance.
- Using the term “power” the performance of 4 different interrupter plates was compared and the 2HL plate performed the best.
- There are several competing factors related to the pulsation performance of a given interrupter plate: pulsation frequency, amplitude and average pressure.
- The design of the DBB interrupter plates allows for a wide range of pulsation characteristics to be achieved.
- The performance of a plate design can be predicted accurately assuming that there are no design flaws or operation faults such as plate bending or debris build up using the pressure-area codes.
- While the research relating low frequency vibrations and fluid pulsations to increased bit cleaning and ROP is currently sparse, in the future this information could be used to

select a plate geometry based on the required operating conditions and lithology of the formations being drilled. This could further increase the performance of the DBB beyond what has been demonstrated by similar designs.

REFERENCES

Babapour, S., & Butt, S. D. (2014, August 18). Investigation of Enhancing Drill cuttings Cleaning and Penetration Rate Using Cavitating Pressure Pulses. American Rock Mechanics Association.

Barton, S. P., Baez, F., & Alali, A. (2011, January 1). Drilling Performance Improvements in Gas Shale Plays using a Novel Drilling Agitator Device. Society of Petroleum Engineers. doi:10.2118/144416-MS

Block, G., & Jin, H. (2009, January 1). Role of Failure Mode on Rock Cutting Dynamics. Society of Petroleum Engineers. doi:10.2118/124870-MS

Boll, S. F. (1979). Suppression of acoustic noise in speech using spectral subtraction. Acoustics, Speech and Signal Processing, IEEE Transactions on, 27(2), 113-120.

Brault, J. W., & White, O. R. (1971). The analysis and restoration of astronomical data via the fast Fourier transform. Astronomy and Astrophysics, 13, 169.

Cheatham, J. B., & Yarbrough, J. G. (1964, March 1). Chip Removal by a Hydraulic Jet. Society of Petroleum Engineers. doi:10.2118/782-PA

Dataq. "What You Really Need to Know About Sample Rate." Dataq Instruments, 2011. Web. 3 Mar. 2016.

Fear, M. J., Abbassian, F., Parfitt, S. H. L., & McClean, A. (1997, January 1). The Destruction of PDC Bits by Severe Slip-Stick Vibration. Society of Petroleum Engineers. doi:10.2118/37639-MS

Fu, J., Li, G., Shi, H., Niu, J., & Huang, Z. (2012, September 1). A Novel Tool to Improve the Rate of Penetration--Hydraulic-Pulsed Cavitating-Jet Generator. Society of Petroleum Engineers. doi:10.2118/162726-PA

Garnier, A. J., & van Lingen, N. H. (1959, January 1). Phenomena Affecting Drilling Rates at Depth. Society of Petroleum Engineers.

Geiger, R. L., & Sanchez-Sinencio, E. (1985). Active filter design using operational transconductance amplifiers: a tutorial. Circuits and Devices Magazine, IEEE, 1(2), 20-32.

Gensheng, L. ,Zhonghou, S., Changshan, Z.,Debin, Z. & Hongbing, C. (2005). Investigation and Application of Self-Resonating Cavitating Water Jet in Petroleum Engineering. Petroleum Science and Technology. doi:10.1081/ LFT-20009686218

Herrington, D., Barton, S. P., & Powell, S. W. (2013, October 22). Step Change Technology Amplifies Vertical Force Applied to Formation at the Bit Enhancing Cutting Efficiency. Society of Petroleum Engineers. doi:10.2118/165926-MS

Hudgins, T. A. (1975, January 1). Pump-Off Control, The Average Motor, Current Method. Society of Petroleum Engineers. doi:10.2118/5331-MS

Kendall, H. A., & Goins, W. C. (1960, January 1). Design and Operation of Jet-Bit Programs For Maximum Hydraulic Horsepower, Impact Force or Jet Velocity. Society of Petroleum Engineers.

Kolle, J. J. (1996, January 1). The Effects of Pressure and Rotary Speed on the Drag Bit Drilling Strength of Deep Formations. Society of Petroleum Engineers. doi:10.2118/36434-MS

Kollé, J. J. (2000, January 1). Increasing Drilling Rate in Deep Boreholes by Impulsive Depressurization. American Rock Mechanics Association.

Leonov, Eugeniy G., and Valeriy I. Isaev. Applied Hydroaeromechanics in Oil and Gas Drilling. Oxford: Wiley-Blackwell, 2009. Print.

Li G. , Shen Z. , Zhou C. , Zhang D. & Chen H. (2005). Petroleum Science and Technology. doi:10.1081/LFT-20009686218

Li, H., Butt, S., Munaswamy, K., & Arvani, F. (2010, January 1). Experimental Investigation of Bit Vibration On Rotary Drilling Penetration Rate. American Rock Mechanics Association.

Liangganga, L., Binga, Z., Qiangb. L. (2014, May 25). Study of Vibration Frequency and Rock Fragmentation Effect of Sonic Drill Rig. Geological Engineering Drilling Technology Conference.

Liz-Losada, R. J., & Alejano, L. R. (2000, January 1). New Safe Mud Weight Window Representations to Prevent Wellbore Instability. Society of Petroleum Engineers. doi:10.2118/62800-MS

Gefei, L. "Torque and Drag - Nuts and Bolts." Pegasus Vertex Inc Blog. Pegasus Vertex, Ltd., 22 Dec. 2015. Web. 31 Mar. 2016.

Longlian C., Haige W., Fucheng Z., Wenxin B. (2013). Pulsed Jet to Improve ROP in Drilling Deep Well. 2013 WJTA-IMCA Conference and Expo.

McLean, R. H. (1964, November 1). Crossflow and Impact Under Jet Bits. Society of Petroleum Engineers. doi:10.2118/889-PA

Mirhaj, A., Kaarstad, E., & Aadnoy, B. S. (2010, January 1). Minimizing Friction In Shallow Horizontal Wells. Society of Petroleum Engineers. doi:10.2118/135812-MS

Prasad, U. (2009, January 1). Drillability of a Rock In Terms of Its Physico-Mechanical And Micro-Structural Properties. American Rock Mechanics Association.

Renshaw, C. E., Golding, N., & Schulson, E. M. (2011, January 1). Systematic Experimental Investigation of the Impact of Increasing Confinement On Shear Faulting. American Rock Mechanics Association.

Scari, A.S, Pockszevnicki, B.C., Landre, J., and Magalhaes, P., (2014) Stress-Strain Compression of AA6082-T6 Aluminum Alloy at Room Temperature. doi:10.1155/2014/387680

Skyles, L., Amiraslani, Y., & Wilhoit, J. (2012, January 1). Converting Static Friction to Kinetic Friction to Drill Further and Faster in Directional Holes. Society of Petroleum Engineers. doi:10.2118/151221-MS

Smalling, D. A., & Key, T. A. (1979, January 1). Optimization Of Jet-Bit Hydraulics Using Impact Pressure. Society of Petroleum Engineers. doi:10.2118/8440-MS

Sutko, A. A. (1973, August 1). Drilling Hydraulics-A Study of Chip Removal Force Under a Full-Size jet Bit. Society of Petroleum Engineers. doi:10.2118/3985-PA

The Editors of Encyclopædia Britannica. "Ohm's Law." Encyclopedia Britannica Online. Encyclopedia Britannica, 2014. Web. 3 Mar. 2016.

Warren, T. M. (1989, December 1). Evaluation of Jet-Bit Pressure Losses. Society of Petroleum Engineers. doi:10.2118/17916-PA

Warren, T. M., & Smith, M. B. (1985, August 1). Bottomhole Stress Factors Affecting Drilling Rate at Depth. Society of Petroleum Engineers. doi:10.2118/13381-PA

Wei, L., Tie, Y., Siqi, L., Xiaoning, Z. (2013). Rock fragmentation mechanisms and experimental study of drilling tools during high-frequency harmonic vibration. doi 10.1007/s12182-013-0268-3

Weisstein, Eric W. "Circle-Circle Intersection." From MathWorld--A Wolfram Web Resource. http://mathworld.wolfram.com/Circle-CircleIntersection.html

Weisstein, Eric W. "Fast Fourier Transform." From MathWorld--A Wolfram Web Resource. http://mathworld.wolfram.com/FastFourierTransform.html

Wells, M. R. (1989, June 1). Dynamics of Rock-Chip Removal by Turbulent Jetting. Society of Petroleum Engineers. doi:10.2118/14218-P

APPENDICES

Data Filtering Code:

```
function [X, f, y, y2, Xave] = fftf(t, x, file, ave, tlim1,
tlim2, varargin)
% fftf - fft filter;
% Base code by Shmuel Ben-Ezra, Ultrashape ltd. August 2009
% Edited by Nick Thorp, Oklahoma State University. September 2015.


%% Verifying input
if ~any(size(t)==1),
   disp('Unexpected vector size! - should be 1D vectors.')
   return
end
if ~any(size(x)==1),
   disp('Unexpected vector size! - should be 1D vectors.')
   return
end
if length(t)~=length(x),
   disp('Unexpected vector size! - should be same length.')
   return
end
%% Definitions
Fs=1/(t(2)-t(1)); %sampling
freq N=length(x);
Nfft=2^nextpow2(N);
f=Fs/2*linspace(0,1,1+Nfft/2); % create freqs
vector cutoff_freq=Fs/8;
my_freqs=[];
if nargin>2,
    cutoff_freq=varargin{1};
end
if nargin>3,
    my_freqs=varargin{2};
end


%% main
y=fft(x,Nfft)/N; % perform fft transform
y2=filterfft(f, y, cutoff_freq, my_freqs); % filter
amplitudes X=ifft(y2); % inverse transform
X=X(1:N)*N;
ind1 = find(y2(1:1+Nfft/2)); % get the nonzero elements in
y2 nf1 = length(ind1); % count nonzero elements


%Smooth Spectrum
[Y2]=moving(y,ave);
```

```
%convert voltage to pressure (psi)
x=((x/560)-0.004)*(3000/16)*1000;
X=((X/560)-0.004)*(3000/16)*1000;


%% display
figname = 'fftf - FFT at work';
ifig = findobj('type', 'figure', 'name',
figname); if isempty(ifig),
    ifig = figure('name', figname);
end
figure(ifig);


plot(X(4270:6270))
hold on

% first plot
ax1 = subplot(3,1,1);
plot(t,x)
hold on
xlim(ax1,[tlim1
tlim2]) xlabel('Sec')
title(strcat( 'Original signal','
"',file,'"')) %second plot
ax2 = subplot(3,1,2);
yplot=abs(Y2(1:1+Nfft/2));
yplot=yplot/max(yplot);
semilogy(f, yplot, f(ind1), yplot(ind1),
'.r'); xlim(ax2,[0 13])
xlabel('Hz')
title(['Smoothed Frequency Spectrum Amplitudes (m=',
num2str(ave),')']) legend('full spectrum', 'selected frequencies')
% third plot
ax3 = subplot(3,1,3);
plot(t,X)
xlim(ax3,[tlim1 tlim2])
xlabel('Sec') %Calculate
X metrics Xave=mean(X);
Std=std(X);
X1=mean(X(5000:10000));
X2=mean(X((N- 5000):N));
Drift=X2-X1;


%Plot Titles
if isempty(cutoff_freq),
    scutoff='No cutoff.';
else
    scutoff=sprintf('Cutoff = %g [hz]', cutoff_freq);
end
stitle3=sprintf('Reconstructed signal with %d selected
frequencies; %s', nf1, scutoff);
title(stitle3)
return


function y2=filterfft(f, y, cutoff,
wins) nf=length(f);
```

```
ny=length(y);
if ~(ny/2+1 == nf),
    disp('unexpected dimensions of input
    vectors!') y2=-1;
    return
end


% cutoff  filter
y2=zeros(1,ny);
if ~isempty(cutoff)
    ind1=find(f<=cutoff);
    y2(ind1) = y(ind1); % insert required elements
else
    y2=y;
end

% dominant freqs filter
if ~isempty(wins),
    temp=abs(y2(1:nf));
    y2=zeros(1,ny);
    for k=1:wins,   % number of freqs that I want
        [tmax, tmaxi]=max(temp);
        y2(tmaxi) = y(tmaxi); % insert required element
        temp(tmaxi)=0; % eliminate candidate from list
    end
end


% create a conjugate symmetric vector of
amplitudes for k=nf+1:ny,
    y2(k) = conj(y2(mod(ny-k+1,ny)+1)); % formula from the help of ifft
end
return

function [y]=moving(x,m,fun)
%MOVING will compute moving averages of order n (best taken as odd)
%
%Usage: y=moving(x,n[,fun])
%where x    is the input vector (or matrix) to be smoothed.
%      m is number of points to average over (best odd, but even
works)
%      y is output vector of same length as x
%      fun  (optional) is a custom function rather than moving averages
%
% Note:if x is a matrix then the smoothing will be done 'vertically'.
%
%
% Example:
%
% x=randn(300,1);
% plot(x,'g.');
% hold on;
% plot(moving(x,7),'k');
% plot(moving(x,7,'median'),'r');
% plot(moving(x,7,@(x)max(x)),'b');
% legend('x','7pt moving mean','7pt moving median','7pt moving
max','location','best')
```

```
%
% optimized Aslak Grinsted jan2004
% enhanced Aslak Grinsted Apr2007


if m==1
    y=x;
    return
end
if size(x,1)==1
    x=x';
end


if nargin<3
    fun=[];
elseif ischar(fun)
    fun=eval(['@(x)' fun '(x)']);
end

if isempty(fun)

    f=zeros(m,1)+1/m;
    n=size(x,1);
    isodd=bitand(m,1);
    m2=floor(m/2);



    if (size(x,2)==1)
        y=filter(f,1,x);
        y=y([zeros(1,m2-1+isodd)+m,m:n,zeros(1,m2)+n]);
    else
        y=filter2(f,x); y(1:(m2-
        ~isodd),:)=y(m2+isodd+zeros(m2-~isodd,1),:); y((n-
        m2+1):end,:)=y(n-m2+zeros(m2,1),:);
    end

else
    y=zeros(size(x));
    sx=size(x,2);
    x=[nan(floor(m*.5),sx);x;nan(floor(m*.5),sx)];
    m1=m-1;
    for ii=1:size(y,1);
        y(ii,:)=fun(x(ii+(0:m1),:));
    end

end

return
```

Area Modelling Code:

```
%Calculates the flow area for different plate designs
%Based on overlapping circles with a linear translation assumption
%Written by Nick Thorp, Oklahoma state University. November 2015.


clear
all clc


    %User Inputs
     delta_t=.001;   %time step
     freq=0.563;     %shaft frequency, hz (from data)
     r=0.25;         %hole radius, in
     Q=420;          %flowrate, GPM
     density=8.33;   %mud density, ppg
     r0=0.21;        %center nozzle radius, in
     Plate=2;        %Plate to model (10 plots all plates)

    %Bit Hole Modeling

    R=0.937;            %radius of hole center to plate center, in
    D=2*pi*R;           %diameter of hole center ring, in
    v=D*freq;           %hole center velocity, in/s
    s=(D-5*2*r)/5;      %linear space between hole edges, in
    tlim=round(1/freq/delta_t);
    Cc=1;               %average pressure correction factor
    A0=(2*pi*r0^2)*Cc;  %null flow area, in^2

    %Plate Design
    if (Plate==0 || Plate==10);
        %Old Plate
        holes=2;                %#holes in plate
        distance=D/5;           %distance between holes
        stagger=distance/v;     %stagger between holes, sec
  nc=(D-(4*5*r))/5;               %distance of "no contact" for each hole
pass, in
        l=nc+4*r;               %length of one hole pass (1/5
revolution), in
        t1=round(1/freq/5);     %time for one hole pass (1/5
revolution), sec
        tnc=nc/v;               %time for "no contact" for one hole
pass, sec
        tc=(t1-tnc);            %time for "contact" for one hole pass,
sec
        tlim=round(1/freq/delta_t);    %time for 1 revolution, s
        Cd=0.61;                %nozzle coefficient


        %Generate time vector for one hole (1/5
        rev) t=zeros([(t1/delta_t)+1,1]);
        for i = 2:1:((t1/delta_t)+1)
            t(i)=t((i-1))+delta_t;
        end


        %Generate distance vector for one hole (1/5 rev)
```

```
d=zeros([(t1/delta_t)+1,1]);
d(1)=2*r+3/2*nc;
x=zeros([(t1/delta_t)+1,1]);
x(1)=0;
for i = 2:1:((t1/delta _t)+1)
    if d(i-1)>0.00001
        d(i)=(1/2*nc+2*r)-(t(i)*v);
    else
        j=i;
        d(i)=abs(d(i));
        x(i)=x(i-
        1)+delta_t*v; break
    end
end


for i = 2:1:((t1/delta_t)+1)
    x(i)=x(i-1)+delta_t*v;
end



for i=(j+1):1:((t1/delta_t)+1)
    d(i)=d(i-1)+delta_t*v;
end



%Area calculations
    %initialize vectors
    Asector=zeros([(t1/delta_t)+1,1]);
    Atriangle=zeros([(t1/delta_t)+1,1]);
    A=zeros([(t1/delta_t)+1,1]);
    P=zeros([(t1/delta_t)+1,1]); A(1)=A0;

for i = 2:1:((t1/delta_t)+1)
    if abs(d(i))<=(2*r)
        %enter area calculations
        Asector(i)=abs((2*pi*r^2/(2*pi))*acos(d(i)/(2*r)));
        Atriangle(i)=abs(d(i)/2*(r^2-(d(i)^2/4))^.5);
        A(i)=A0+holes*2*(Asector(i)-Atriangle(i)); %pressure
        calculation P(i)=Q^2*density/(12031*Cd^2*A(i)^2);

        P(1)=P(2);
    else
        A(i)=A0;
        P(i)=Q^2*density/(12031*Cd^2*A(i)^2);
    end
end



%simulate 1 revolution
Pt=zeros((tlim),2); for
i=2:1:(tlim)
    Pt(1,1)=0; Pt(i,1)=Pt(i-
    1,1)+delta_t;
end
```

```
    j=0;
    for i=1:1:t1/delta_t
        Pt(i,2)=P(i-j+1);

    end
    j=i;
    for i=j:1:j+t1/delta_t
        Pt(i,2)=P(i-j+1);

    end
    j=i;
    for i=j:1:j+t1/delta_t
        Pt(i,2)=P(i-j+1);

    end
    j=i;
    for i=j:1:j+t1/delta_t
        Pt(i,2)=P(i-j+1);

    end
    j=i;
    for i=j:1:j+t1/delta_t
        Pt(i,2)=P(i-j+1);

    end
    j=i;
    plot(Pt(:,1),Pt(:,2),'r')
hold on
meanpressure=mean(Pt(:,2)) end



if (Plate==1 || Plate==10);
    %1 Hole Plate
    Cd=0.48;         %nozzle coefficient

    Aone=A0+3*r^2*pi;
    oneholeP=Q^2*density/(12031*Cd^2*Aone);
    Pt=zeros([1/freq,2]);
    for i = 1:1:((1/freq/delta_ t)) Pt(i,1)=(i-
        1)*delta_t;
        Pt(i,2)=Q^2*density/(12031*Cd^2*Aone^2);
    end
    plot(Pt(:,1),Pt(:,2),'g')
    hold on
end




if (Plate==2 || Plate==10);

    %2 Hole Plate
```

```
        holes=2;                            %#holes in plate
        t1=round(1/freq/5/delta_t);         %#time for 1/5th revolution
(ms)
        Cd=0.95;                            %nozzle coefficient
        l=0.5*r;                            %length of hole center
extension(not used)

        %Generate time vector for one hole (1/5
        rev) t=zeros([t1,1]);
        t(1)=delta_t;
        for i = 2:1:t1
            t(i)=t((i-1))+delta_t;
        end

        %Calculate starting area for one
        hole d_0=r;
        A_0=2*((2*pi*r^2/(2*pi))*acos(d_0/(2*r))-
(d_0/2)*(r^2-((d_0^2)/4))^.5);

        %create distance vector for fully open to half
        open d(1)=2*r;
        for i = 2:1:(r/v/delta_t)
            d(i)=d((i-1))-v*delta_t;
            if (d(1)+d(i))<0
                    break
            end
        end



        %Beginning and end area change

        %closing hole
        for i=2:round((r)/v/delta_t)
            dc(1)=(r);
            closing(1)=A_0;
            dc(i)=dc(i-1)+v*delta_t;
            closing(i)=2*((2*pi*r^2/(2*pi))*acos(dc(i)/(2*r))-
(dc(i)/2)*(r^2-((dc(i)^2)/4))^.5);
            if dc(i)>(2*r)
                break
            end
        end



        %openning hole
        for i=2:round((r)/v/delta_t)
            dd(1)=(r); dd(i)=dd(i-1)
            -v*delta_t; dp(1)=(2*r);
            openning(1)=0;
            dp(i)=dp(i-1)-v*delta_t;

            openning(i)=2*((2*pi*r^2/(2*pi))*acos(dp(i)/(2*r))-
(dp(i)/2)*(r^2-((dp(i)^2)/4))^.5);
            aoc(1)=A_0;
            aoc(i)=closing(i)+openning(i);
```

```
            if dp(i)>(2*r)
                break
            end
        end
            j=i;
        %reverse it for
        openning dr=fliplr(dd);

        %Area calculations open
        hole dm=0;
        am_0=2*((2*pi*r^2/(2*pi))*acos(dm/(2*r))-
(dm/2)*(r^2-((dm^2)/4))^.5);


        %combine area vectors and calculate
        pressure A=zeros([t1,1]);

        for i=1:j
            A(i)=aoc(i);
        end
        for i=(j+1):(2*j) A(i)=2*((2*pi*r^2/(2*pi))*acos(dd(i-
            j)/(2*r))-(dd(i-
j)/2)*(r^2-((dd(i-
        j))^2)/4)^.5); end
        for i=(2*j+1):(t1-
            2*j) A(i)=am_0;
        end
        for i=(t1-2*j+1):(t1-j-1) A(i)=2*((2*pi*r^2/(2*pi))*acos(dr(i -
            (t1-2*j))/(2*r))-(dr(i-
(t1-2*j))/2)*(r^2-((dr(i-(t1-
        2*j)))^2)/4)^.5); end
        for i=(t1-j):t1-1
            A(i)=aoc(i- (t1-
            j)+1); A(t1)=A_0;
        end

        %Add in open flow area
        (null) for i=1:t1
            A(i)=holes*A(i)+A0;
        end

        %pressure calculation
        for i=1:t1
            P(i)=Q^2*density/(12031*Cd^2*A(i)^2);
            P(i)=Q^2*density/(12031*Cd^2*A(i)^2);
        end

        %simulate 1 revolution
        Pt=zeros((tlim),2); for
        i=2:1:(tlim)
            Pt(1,1)=delta_t;
            Pt(i,1)=Pt(i-1,1)+delta_t;
        end
```

```
    j=0;
    for i=1:1:(t1)
        Pt(i,2)=P(i-j);

    end
    j=i;
    for i=j+1:1:j+(t1)
        Pt(i,2)=P(i-j);

    end
    j=i;
    for i=j+1:1:j+(t1)
        Pt(i,2)=P(i-j);

    end
    j=i;
    for i=j+1:1:j+(t1)
        Pt(i,2)=P(i-j);

    end
    j=i;
    for i=j+1:1:j+(t1)
        Pt(i,2)=P(i-j);

    end
    j=i;
    plot(Pt(:,1),Pt(:,2))
    xlim([0,(tlim*delta_t)]);
    hold on
    %calculate plate design metrics
    meanpressure=mean(Pt(:,2)) %psi
    sd=std(Pt(:,2))

end
```

VITA

Nicholas James Thorp

Candidate for the Degree of

Master of Science

Thesis: CHARACTERIZATION OF A PULSATING DRILL BIT BLASTER

Major Field: Mechanical and Aerospace Engineering

Biographical:

Education:

Completed the requirements for the Master of Science in Mechanical and Aerospace Engineering at Oklahoma State University, Stillwater, Oklahoma in May, 2016.

Completed the requirements for the Bachelor of Science in Mechanical Engineering at Oklahoma State University, Stillwater, Oklahoma in May, 2014.

Experience: NORDAM, Lonestar Aerospace

Professional Memberships: Society of Petroleum Engineers